Lee *et al. Cellular & Molecular Biology Letters* (2025) 30:59
https://doi.org/10.1186/s11658-025-00735-5

Cellular & Molecular Biology Letters

RESEARCH ARTICLE Open Access

# Narciclasine enhances cisplatin-induced apoptotic cell death by inducing unfolded protein response-mediated regulation of NOXA and MCL1

Ji Hae Lee[1,2], Seung Hee Seo[1], Jaegal Shim[1], Yong-Nyun Kim[1] and Kyungsil Yoon[1*]

*Correspondence:
kyoon@ncc.re.kr

[1] Cancer Metastasis Branch, Research Institute, National Cancer Center, Goyang 10408, South Korea
[2] College of Pharmacy, Graduate School of Pharmaceutical Sciences, Ewha Womans University, Seoul 03760, South Korea

## Abstract

**Background:** Platinum-based chemotherapy is commonly used to treat non-small cell lung cancer (NSCLC); however, innate and acquired resistance is clinically seen in many patients. Hence, a combinatorial approach with novel therapeutic agents to overcome chemoresistance is a promising option for improving patient outcomes. We investigated the combinational anticancer efficacy of cisplatin and narciclasine in three-dimensional NSCLC tumor spheroids.

**Methods:** To assess the efficacy of cisplatin and narciclasine, cell viability assays, live/dead cell staining, cell death enzyme-linked immunosorbent assay (ELISA), western blot analysis for proteins related to apoptosis, and in vivo xenograft experiments were performed. The synergistic effects of cisplatin and narciclasine were elucidated through transcriptomic analysis and subsequent validation of candidate molecules by regulating their expression. To clarify the underlying molecular mechanisms, the activation of unfolded protein responses and kinetics of a candidate protein were assessed.

**Results:** Narciclasine inhibited viability of NSCLC tumor spheroids and augmented the sensitivity of cisplatin-resistant tumor spheroids to cisplatin by inducing apoptosis. After conducting bioinformatic analysis using RNA sequencing data and functional validation experiments, we identified *NOXA* as a key gene responsible for the enhanced apoptosis observed with the combination of cisplatin and narciclasine. This treatment dramatically increased NOXA while downregulating anti-apoptotic MCL1 levels. Silencing NOXA reversed the enhanced apoptosis and restored MCL1 levels, while MCL1 overexpression protected tumor spheroids from combination treatment-induced apoptosis. Interestingly, narciclasine alone and in combination with cisplatin induced unfolded protein response and inhibited general protein synthesis. Furthermore, the combination treatment increased NOXA expression through the IRE1α–JNK/p38 axis and the activation of p53. Cisplatin alone and in combination with narciclasine destabilized MCL1 via NOXA-mediated proteasomal degradation.

**Conclusions:** We identified a natural product, narciclasine, that synergizes with cisplatin. The combination of cisplatin and narciclasine induced NOXA expression, downregulated MCL1, and ultimately induced apoptosis in NSCLC tumor spheroids. Our findings suggest that narciclasine is a potential natural product for combination with cisplatin for treatment of NSCLC.

**Keywords:** Narciclasine, Chemoresistance, Cisplatin, Apoptosis, Tumor spheroids, Non-small cell lung cancer

## Background

Lung cancer has the highest mortality rate among all cancers worldwide, accounting for 21% of all cancer-related deaths. This is attributed to diagnosis at late stages for nearly half of the patients with lung cancer [1, 2]. Non-small cell lung cancer (NSCLC) is the most common type of lung cancer, accounting for approximately 85% of all lung cancer cases [3]. Targeted therapy is one of the treatment options for advanced NSCLC harboring oncogenic driver mutations, while patients without oncogenic driver mutations are treated with immune checkpoint inhibitors, either alone or in combination with chemotherapy or standard chemotherapy [4–9].

Platinum-based drugs are commonly used as chemotherapeutic agents for NSCLC. Cisplatin is frequently combined with other treatment modalities such as surgery, radiation, targeted therapy, or immunotherapy to enhance treatment effectiveness [5, 10, 11]. Although cisplatin-based combination therapy can be effective for the treatment of NSCLC, it has several limitations, namely the development of resistance and toxicity [12, 13]. One approach to overcome these barriers and enhance the efficacy of cisplatin is to explore novel combination strategies that can not only exhibit synergistic anticancer effects and improve patient outcomes but also decrease cisplatin-associated toxicity through dose reduction.

Natural products have long been a valuable source of drugs for the treatment of various diseases, including cancer [14]. To identify a novel combination that can enhance cisplatin sensitivity, we screened a natural product library and identified narciclasine as the most potent candidate. Narciclasine is an isocarbostyril alkaloid derived from the bulbs of several varieties of *Narcissus* and exhibits antitumor activity against breast, gastric, and brain cancers [15–18]. Several mechanisms have been reported to underlie the antitumor effects of narciclasine. Narciclasine inhibits protein synthesis by directly binding to the translation elongation factor eukaryotic elongation factor 1-alpha (eEF1A) [19] and induces autophagy-mediated apoptosis through inhibition of Akt/mammalian target of rapamycin (mTOR) phosphorylation [17]. Narciclasine directly interacts with signal transducer and activator of transcription 3 (STAT3), inhibiting its phosphorylation in MCF-7 cells. Additionally, narciclasine induces reactive oxygen species (ROS), which further contributes to the inhibition of STAT3 in tamoxifen-resistant MCF-7 cells [20]. Overall, narciclasine exerts its antitumor effects through multiple mechanisms of action, making it a promising candidate for cancer therapy.

NOXA, also known as phorbol-12-myristate-13-acetate-induced protein 1 (PMAIP1), is a pro-apoptotic protein belonging to the Bcl-2 homology 3 (BH3)-only family of B-cell lymphoma 2 (BCL2) proteins [21]. BH3-only proteins, including NOXA, PUMA, BID, BAD, BIM, BIK, BMF, and HRK, are activated in response to various cellular

stressors and function as upstream regulators of apoptosis [22]. Specifically, NOXA binds to anti-apoptotic proteins of the BCL2 family, namely myeloid cell leukemia-1 (MCL1) and BCL2-related protein A1 (BCL2A1), neutralizing their ability to suppress BAX/BAK activation and thereby initiating apoptosis [23, 24]. NOXA regulates Mule-dependent ubiquitination of MCL1 by inhibiting the interaction between ubiquitin specific peptidase 9X-linked and MCL1, ultimately inducing MCL1 degradation [25]. Erlotinib-induced NOXA promotes mitochondria-associated ubiquitin E3 ligase MARCH5-mediated degradation of MCL1 [26]. Additionally, NOXA is required for cisplatin-induced phosphorylation of MCL1, which results in proteasome-dependent degradation, ultimately leading to induction of apoptosis [27]. Hence, the balance between NOXA and MCL1 determines the susceptibility of cells to apoptosis and also plays a critical role in tumor pathogenesis and progression, as well as therapeutic resistance [28, 29]. Therefore, targeting BCL2 family members is a promising approach for cancer treatment.

In the present study, we investigated the synergistic antitumor effects of cisplatin and narciclasine using NSCLC tumor spheroids and their mechanism of action, specifically in the regulation of anti-apoptotic MCL1.

## Materials and methods

### Reagents

Narciclasine (HY-16563), MG-132 (HY-13259), KIRA6 (HY-19708), GSK2606414 (HY-18072), SP600125 (HY-12041), and SB203580 (HY-10256) were purchased from MedChemExpress (USA). Dimethyl sulfoxide was used as a vehicle control. Cycloheximide (01810), puromycin (P8833), *N*-acetylcysteine (A7250), and glutathione ethyl ester (G1404) were purchased from Sigma-Aldrich (USA). Cycloheximide and puromycin were dissolved in methanol and water, respectively. Cisplatin was obtained from Dong-A Pharmaceutical Co. Ltd (Korea).

### Cell line and cell culture

A549, NCI-H460, NCI-H1975, and NCI-H358 cells were purchased from the American Type Culture Collection (USA), and HCC2279 (KCLB no. 72279) was purchased from Korea Cell Line Bank (Korea). All cancer cell lines were cultured in Roswell Park Memorial Institute (RPMI) 1640 supplemented with penicillin (100 units/ml), streptomycin (100 μg/ml), and 10% fetal bovine serum at 37 °C with 5% $CO_2$. To generate tumor spheroids, the following cell lines were seeded into a cell floater 96-well round-bottomed plate (34896, SPL, Korea) and centrifuged for 10 min at 1000 rpm: A549, HCC2279, and NCI-H1975 at $5\times10^4$ cells/well, NCI-H460 at $2\times10^4$ cells/well, and NCI-H358 at $6\times10^4$ cells/well. Tumor spheroids were cultured in RPMI 1640 culture medium with 0.5% Matrigel for A549, NCI-H358, and NCI-H460, and with 2% Matrigel for H1975 and HCC2279 (BD Biosciences, USA) to promote compact spheroid formation. Compounds were treated 2 days after formation of tumor spheroids.

### Three-dimensional (3D) cell viability assay and combination index (CI) calculation

The viability of tumor spheroids was determined using CellTiter-Glo® 3D cell viability assay (Promega, USA) according to the manufacturer's protocol. Luminescence was

measured by the GloMax-Multi Detection System (Promega, USA). The synergistic effects of cisplatin and narciclasine were determined by calculating the combination index (CI) using CalcuSyn software. A CI value less than 1 represents synergism.

#### Western blot analysis

Cell lysates were prepared in radio immunoprecipitation assay (RIPA) buffer (89900, Thermo Scientific, USA), supplemented with protease inhibitor cocktail, phosphatase inhibitor (Calbiochem, USA), and phenylmethylsulfonyl fluoride (PMSF). Protein concentrations were determined using a bicinchoninic acid (BCA) protein assay kit (Thermo Scientific, USA). Equal amounts of protein were separated by 8–15% sodium dodecyl sulfate–polyacrylamide gel electrophoresis (SDS-PAGE) and transferred to a polyvinylidene fluoride (PVDF) membrane (Millipore, USA). Antibodies against β-actin (sc-477778), p53 (sc-126), and BCL2 (sc-509) were purchased from Santacruz Biotechnology. Antibodies against cleaved caspase-7 (#9491), cleaved PARP (#9541), cleaved caspase-9 (#9505), caspase-9 (#9502), caspase-8 (#9746), GAPDH (#2118), NOXA (#14766), MCL1 (#4572), BCL2A1 (#14093), ATF3 (#18665), survivin (#2808), phospho-eIF2α (#3398), eIF2α (#5324), PERK (#5683), phospho-4E-BP (#2855), IRE1α (#3294), phospho-JNK (#4668), JNK (#9252), phospho-p38 (#4511), p38 (#8690), CHOP (#2895), phospho-STAT1 (#8826), STAT1 (#9172), and His (#2366) were purchased from Cell Signaling. Antibodies against MAFF (GTX120264) and 4E-BP1 (GTX109162) were purchased from GeneTex. Antibody against BTG3 (NBP1-89098) was from Novus Biologicals and FLAG (#F7425) was from Sigma-Aldrich. Antibody against phospho-IRE1α (PA1-16927) was from Invitrogen, and Vinculin (PM088) was from MBL. Secondary antibodies, goat anti-mouse IgG HRP (SA001-500) and goat anti-rabbit IgG HRP (SA002-500), were obtained from GenDEPOT.

#### Live/dead cell staining

Tumor spheroids were stained using the LIVE/DEAD™ viability/cytotoxicity kit (Thermo Scientific, USA) according to the manufacturer's protocol. Briefly, tumor spheroids were stained with 1 μM calcein-acetoxymethyl ester (AM) and 10 μM ethidium homodimer-1 (EthD-1) for 20 min at 37 °C. Images were captured with an Operetta High Content Screening System (PerkinElmer, USA) and analyzed with Harmony 3.5.2 software. The dead cell area (%) was quantified using the following formula:

$$\text{Dead cell area (\%)} = (\text{dead cell area}/(\text{live cell area} + \text{dead cell area})) \times 100.$$

#### Apoptosis analysis by flow cytometry

Apoptosis was measured using the BD Pharmingen PE annexin V apoptosis detection kit. Tumor spheroids were dissociated into single cells using 0.2% trypsin–ethylenediaminetetraacetic acid (EDTA) for 5 min at 37 °C. Cells were suspended in annexin V-binding buffer at $1\times10^5$ cells/100 μL, stained with PE annexin V and 7-amino-actinomycin (7-AAD) for 15 min, and analyzed by flow cytometry. Cells undergoing early apoptosis, indicated by PE annexin V positivity and 7-AAD negativity, are represented graphically.

### Apoptosis analysis by ELISA

Apoptosis was evaluated using the Cell Death Detection ELISAPlus kit (Roche, Germany) according to the manufacturer's protocol by quantifying cytoplasmic histone-complexed DNA fragments (mono- and oligonucleosomes). Absorbance was measured at 405 nm with a reference wavelength of 490 nm using a GloMax-Multi detection system (Promega, USA).

### Xenograft mouse model

Five-week-old male BALB/c nude mice were purchased from Orient Bio (Korea) and acclimated for 7 days. A549 ($5 \times 10^6$) cells were suspended in 100 μL phosphate-buffered saline and mixed with 50 μL Matrigel (BD Biosciences). The cells were subcutaneously injected into 6-week-old BALB/c nude mice under isoflurane (JW Pharmaceutical, Korea) anesthesia. When the tumor size reached 60–70 $mm^3$, the mice were divided randomly into four groups. Vehicle (saline solution), cisplatin (2 mg/kg), and narciclasine (1 mg/kg) were injected intraperitoneally twice weekly in 100 μL volume of each injection. Tumor diameters were measured twice a week up to 4 weeks, and the volume was calculated with the following formula: $V(mm^3) = \text{length} \times \text{width} \times \text{width}/2$. Mice were sacrificed before the tumor volume exceeded 1000 $mm^3$.

### RNA-sequencing and data analysis

Tumor spheroids were treated with cisplatin, narciclasine, or both for 24 h, and total RNA was extracted using the RNeasy Mini Kit (Qiagen, Germany). RNA quality was evaluated using the Agilent 2100 Bioanalyzer (Agilent Technologies, Netherlands). QuantSeq 3′ mRNA sequencing was commercially commissioned to Ebiogen Inc. (Korea). The mRNA libraries were prepared using the QuantSeq 3' mRNA-Seq Library Prep Kit (Lexogen, Austria) according to the manufacturer's instructions and sequenced in 75-bp single-end reads on the NextSeq 500 (Illumina, USA). Differentially expressed genes (DEGs) with fold change of $\geq 2$ were identified using Excel-based DEG analysis software (ExDEGA, Ebiogen, Korea). Gene set enrichment analysis (GSEA) was performed to identify enriched gene sets using GSEA software (version 4.0.3, Broad Institute, USA). The hallmark gene sets from the Molecular Signatures Database (MSigDB) were utilized. Gene sets with a false discovery rate (FDR) $q < 0.1$ and nominal $p < 0.01$ were considered significant.

### Transfection and RNAi

Cells were transfected with 20 nM of siRNA using Lipofectamine RNAiMAX transfection reagent (Invitrogen, USA) following the manufacturer's protocol. The sequences of siRNA were as follows: *NOXA* siRNA, 5′-GGUGCACGUUUCAUC AAUU-3′; *p53* siRNA #1 5′-CACUACAACUACAUGUGUA-3′, #2 5′-UGAGGU UGGCUCUGACUGU-3′; *ATF3* siRNA #1 5′-GGAGUCCUCAUUGAAUCCU-3′, #2 5′-CACAAGGACGUCGGCUACU-3′; *MCL1* siRNA #1 5′-CAGAACGAAUUGAUG UGUA-3′, #2 5′-UGUUCAGUUCUAGAGUGUA-3′; *Survivin* siRNA #1 5'-GAC UUGGCCCAGUGUUUCU-3′, #2 5′-GCAUCUCUACAUUCAAGAA-3′; *GADD45A*

siRNA, 5′-GUAGUUACUCAAGCAGUUA-3′; *MAFF* siRNA, 5′-CCAGCAAAG CUCUAAAGAU-3′; *PHLDA2* siRNA, 5′-GUGUACUUCACCAUCGUCA-3′; *EGR1* siRNA, 5′-ACGACAGCAGUCCCAUUUA-3′; *TUBB2A* siRNA, 5′-CACACU GUUGAUGUAAUGA-3′; *BCL10* siRNA, 5′-GAAAUUUCUUGUCGAACAU-3′; *GADD45B* siRNA, 5′-GUUGAUGAAUGUGGACCCA-3′; *BTG3* siRNA, 5′-UUG AGAGGUUUGCUGAGAA-3′; *ID2* siRNA, 5′-CAAGAAGGUGAGCAAGAUG-3′. Negative control siRNA was purchased from Bioneer (Korea). For siRNA-transfected tumor spheroids formation, cells were replated in a 96-well round-bottomed plate 6 h post-transfection. His-tagged control or ubiquitin plasmids were transfected into A549 cells using Lipofectamine 2000 (Invitrogen, USA).

#### Quantitative real-time PCR

Total RNA was extracted from tumor spheroids using the RNeasy Mini Kit (Qiagen, Germany), and 1 μg of RNA was reverse transcribed using a cDNA synthesis kit (Dyne Bio, Korea). Quantitative polymerase chain reaction (qPCR) was performed using SFC green qPCR master mix (BioFACT, Korea) with the LightCycler 96 real-time PCR system (Roche, Germany). Primer sequences used for PCR were as follows: *NOXA*, (F: CCGGCAGAAACTTCTGAATC and R: CGTGCACCTCCTGAGAAAAC); *MCL1*, (F: CCAAGAAAGCTGCATCGAACCAT and R: CAGCACATTCCTGATGCCACCT); *BIRC5*, (F: TGAGAACGAGCCAGACTTGG and R: TGGTTTCCTTTGCATGGGGT); *MAFF*, (F: CTGTCGGACGAGGCGCTGATG and R: AGCCACGGTTTTTGAGTG TGCG); *BTG3*, (F: TAGTGACCTGGGCTTGCCAAAG and R: CCCTGGTAACTT TCCTGGAGATC); *TP53*, (F: CCTCAGCATCTTATCCGAGTGG and R: TGGATG GTGGTACAGTCAGAGC); *ATF3*, (F: CGCTGGAATCAGTCACTGTCAG and R: CTT GTTTCGGCACTTTGCAGCTG); *GAPDH*, (F: TGCACCACCAACTGCTTAGC and R: GGCATGGACTGTGGTCATGAG). GAPDH was used as an internal control. The relative gene expression was quantified using the $2^{-\Delta\Delta Ct}$ method.

#### Stable cell line generation

The full-length cDNA of human *MCL1* (KU016524) was obtained from the Korea Human Gene Bank and subcloned into a pLenti-c-MYC-DDK-P2A-RFP vector (OriGene, USA), replacing the original puro segment with RFP. To generate cells overexpressing MCL1, pLenti-Ctrl and pLenti-MCL1 vectors were transfected along with pMD2G and psPAX into 293FT cells to produce lentivirus. Medium containing lentivirus particle was applied to A549 cells with 0.8 μg/ml polybrene for 3 days, and cells positive for RFP were sorted by using FACSAria II (BD Biosciences).

#### SUnSET assay

Tumor spheroids were incubated with cisplatin, narciclasine, or the combination for 2 h, followed by 15-min treatment with 5 μg/ml puromycin to label nascent peptides. As a positive control, tumor spheroids were treated with 100 μg/ml cycloheximide for 15 min prior to puromycin treatment. Tumor spheroids were lysed, and puromycin-labeled peptides were detected by western blotting using an anti-puromycin antibody, clone 12D10 (Sigma Aldrich, USA).

### Half-life measurement

After 24 h of transfection with siNC or siNOXA, cells were cultured in fresh medium containing 5 μM cisplatin, 0.1 μM narciclasine, or both. After 24 h, cells were treated with 10 μg/ml cycloheximide for 10, 20, 30, or 40 min and subsequently lysed for western blotting. The bands of MCL1 and GAPDH were scanned, and the intensities of the bands were semiquantified by using ImageJ software. The relative concentration of MCL1 at 10 min that started to be affected by cycloheximide was defined as 1. The intensity of MCL1 band at each indicated time point was normalized by comparing the relative concentration of MCL1 with that at 10 min. The protein half-life was calculated by linear regression analysis. The calculated half-life was averaged for each of three independent experiments.

### Statistical analysis

Statistical analyses were performed using GraphPad Prism 9. Data are presented as mean ± standard deviation (SD) or standard error on the mean (SEM). Comparison between two groups was performed using Student's *t*-test, and multiple comparisons within groups were performed using analysis of variance (ANOVA). Significance was defined as $p < 0.05$.

## Results

### Narciclasine enhances the sensitivity of NSCLC cells to cisplatin

In a preliminary study, we screened a natural product library and identified that narciclasine both alone and in combination with cisplatin considerably inhibited the viability of NSCLC tumor spheroids. Subsequently, we investigated the effects of cisplatin on the viability of NSCLC tumor spheroids and found that A549, NCI-H358, NCI-H1975, and HCC2279 exhibited relative resistance to cisplatin when compared with NCI-H460 (Fig. 1A; Supplementary Fig. S1A, B). Hence, we treated four tumor spheroids (derived from A549, NCI-H358, NCI-H1975, and HCC2279) with various concentrations of cisplatin or narciclasine for 72 h, and determined the half-maximal inhibitory concentration ($IC_{50}$) values from dose–response curves (Fig. 1A, B; Supplementary Fig. S1B). Subsequently, on the basis of the $IC_{50}$ values, we assessed the synergistic effects of the combination of cisplatin and narciclasine at various concentrations and determined the combination index (CI). The decrease in viability of A549 tumor spheroids was more substantial with the combination treatment than with the individual treatments (Fig. 1C). Synergistic effects were observed in A549 tumor spheroids for seven of the nine tested combinations, with a CI of less than 1 (Fig. 1D). Other cell lines also exhibited synergistic effects with most combinations of narciclasine and cisplatin (Supplementary Fig. S2A, B). For subsequent analysis, we chose the lowest set of concentrations (indicated by ▼) that resulted in less than half of the cell viability compared with each treatment (indicated by $) (Figs. 1C; Supplementary Fig. S2A). Hence, thereafter, A549 tumor spheroids were treated with 10 μM of cisplatin and 0.3 μM of narciclasine. To investigate the time-dependent responses to the combination treatment, we assessed cell viability at 24, 48, and 72 h after treatment with the

combination at the selected concentrations. The effects of the combination increased over time not only in A549 tumor spheroids but also in other cell lines (Fig. 1E; Supplementary Fig. S2C).

To confirm whether the inhibition of cell viability by the combination of cisplatin and narciclasine was attributable to increased apoptosis, we verified cleavage of caspase-7, caspase-8, and caspase-9. Cleavage of caspase-7 and caspase-9 was higher with the combination treatment when compared with the individual treatments. On the other hand, there was no difference in the cleavage of caspase-8, which mediates the extrinsic apoptotic pathway, between the cisplatin alone and combination groups (Fig. 1F). Apoptosis was also found to be increased in other NSCLC tumor spheroids treated with the combination (Supplementary Fig. S2D). We also performed cell staining, flow cytometry, and ELISA to further confirm the mechanism of cell death induced by the combination treatment. Staining of A549 tumor spheroids with calcein-acetoxymethyl ester and ethidium homodimer revealed an increase in the number of dead cells as well a decrease in spheroid size in tumor spheroids treated with both cisplatin and narciclasine, when compared with those treated with the individual treatments (Fig. 1G). Flow cytometric analysis of dissociated tumor spheroids stained with annexin V and 7-amino-actinomycin D revealed a considerable increase in the percentage of cells in the early stage of apoptosis with the combination treatment (Fig. 1H; Supplementary Fig. S3). Lastly, we quantified cytoplasmic histone-complexed DNA fragments and observed an increased level of apoptosis in A549 tumor spheroids treated with the combination treatment (Fig. 1I). To confirm our in vitro findings, we evaluated the antitumor activity

(See figure on next page.)

**Fig. 1** Narciclasine significantly enhanced the sensitivity of NSCLC tumor spheroids to cisplatin. **A**, **B** A549 tumor spheroids were treated with various concentrations of cisplatin (**A**) or narciclasine (**B**) for 72 h, and cell viability was determined by measuring cellular adenosine triphosphate (ATP) content. Data are mean ± SD from three independent experiments in triplicate. **C** The viability of tumor spheroids was assessed following cisplatin, narciclasine, or the combination treatment at the indicated concentrations for 72 h. *$p < 0.05$ versus same dose of cisplatin; †$p < 0.05$ versus same dose of narciclasine; $, less than half of cell viability compared with each treatment; ▼, selected combination dose. Data are mean ± SD from three independent experiments in triplicate. **D** Combination index (CI) values calculated using CompuSyn. CI of < 1.0 indicates synergism. **E** Tumor spheroids were treated with the vehicle, 10 μM cisplatin, 0.3 μM narciclasine, or both for the indicated time periods. Images were taken prior to viability assay. *$p < 0.05$ versus cisplatin; †$p < 0.05$ versus narciclasine. Data are mean ± SEM from three independent experiments in triplicate. Scale bar: 100 μm. **F** Whole-cell lysates were prepared from A549 tumor spheroids 48 h after treatment with cisplatin, narciclasine, or the combination. The levels of cleaved caspases were analyzed by western blotting. GAPDH was used as the loading control. Data represent one of three independent experiments with similar results. **G** Tumor spheroids were treated with cisplatin, narciclasine, or the combination for 48 h. Live cells were stained green with calcein-acetoxymethyl ester, whereas dead cells were stained red with ethidium homodimer-1. Images were taken at magnification of 100× using the Operetta high-content analysis system. Scale bar: 200 μm. Results of the quantitative analysis of the dead cell area are shown in the right panel. *$p < 0.05$. Data are mean ± SD from three independent experiments in triplicate. **H** Tumor spheroids were dissociated 48 h after the indicated treatments and analyzed using flow cytometry. Apoptotic cells were presented as percentages of annexin V-positive/7-amino-actinomycin D (7-AAD)-negative cells. *$p < 0.05$. Data are mean ± SEM from three independent experiments in triplicate. **I** A549 tumor spheroids were treated with cisplatin, narciclasine, or the combination for 48 h, and apoptosis was analyzed using a Cell Death Detection ELISA kit capable of detecting mono- and oligonucleosomes. *$p < 0.05$. Data are mean ± SEM from three independent experiments in triplicate. **J** Tumor volume and body weight were measured on the indicated days. $n = 5$ per group. Data are mean ± SEM. *$p < 0.05$. Data represent one of two independent experiments with similar results ($n = 5$ per group for each experiment). **K** The weight of the excised tumors was measured 25 days after cisplatin, narciclasine, or the combination. Data are mean ± SEM. *$p < 0.05$

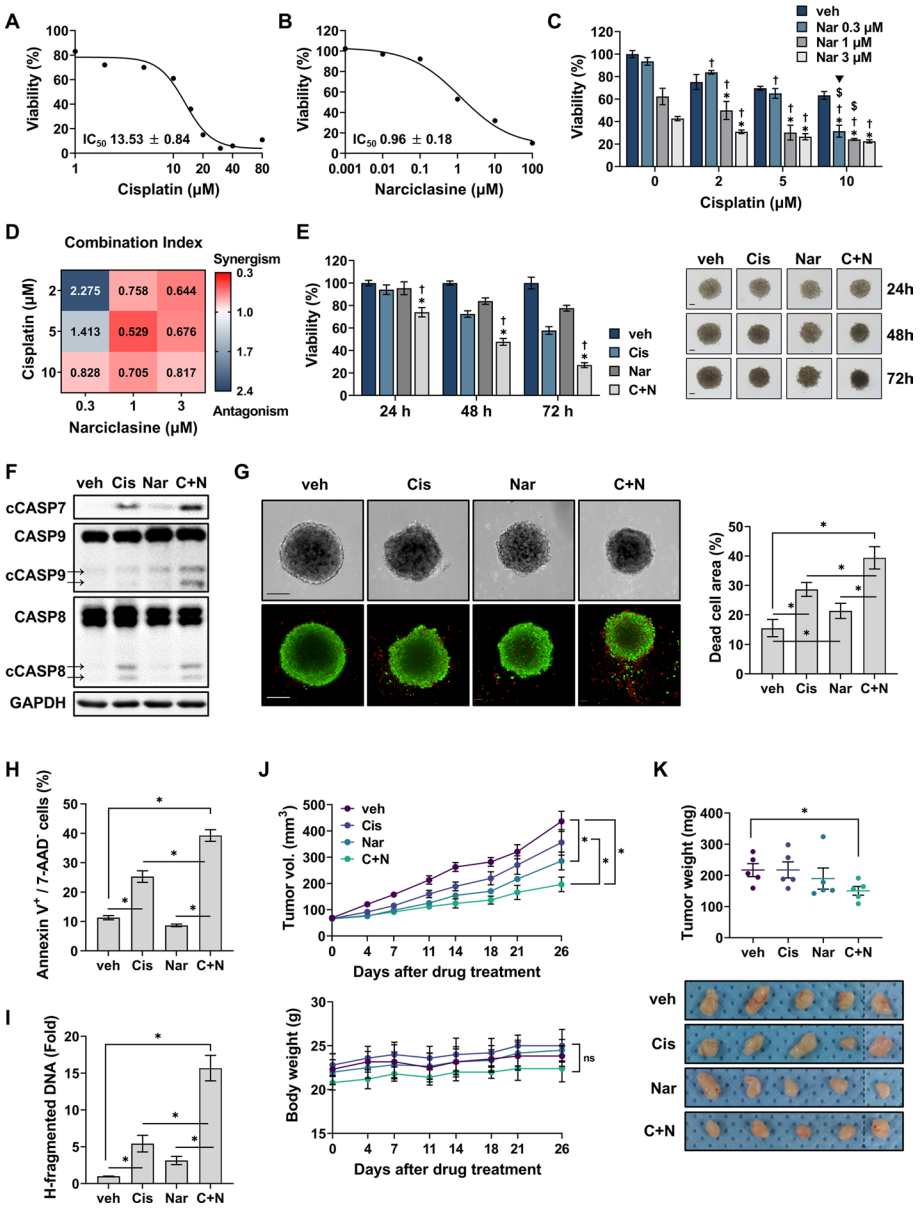


**Fig. 1** (See legend on previous page.)

of the combination of cisplatin and narciclasine in a xenograft mouse model. As shown in Fig. 1J, K, tumor growth and weight were significantly suppressed by the combination treatment when compared with the vehicle. Taken together, these data demonstrate that the combination of cisplatin and narciclasine exhibits potent synergistic effects against NSCLC proliferation both in vitro and in vivo.

### NOXA regulation underlies cisplatin and narciclasine combination treatment-induced apoptosis in NSCLC tumor spheroids

To investigate the mechanism underlying the synergistic effects of cisplatin and narciclasine, we performed RNA sequencing after treatment of A549 tumor spheroids with cisplatin, narciclasine, or the combination of cisplatin and narciclasine for 24 and

48 h. We observed a higher number of genes exhibiting greater than a twofold change in expression in the combination treatment group than in the individual treatment groups (Supplementary Fig. S4A). To select candidate genes that are responsible for the synergistic effects of cisplatin and narciclasine, we performed bioinformatic analysis, integrating differentially expressed gene (DEG) analysis based on changes in gene expression and gene set enrichment analysis (GSEA) for functional gene classification (Fig. 2A). Initially, we selected 335 genes that displayed more than a twofold change in expression across all three comparison groups (combination versus vehicle, combination versus cisplatin, and combination versus narciclasine) with consistent changes at both 24 and 48 h post-treatment. Furthermore, to understand the functional categories of genes that were enriched, we performed GSEA to compare the cisplatin alone and combination groups (Supplementary Fig. S4B). We then selected the core enriched genes included in those gene sets and found 89 upregulated genes and 11 downregulated genes in the combination treatment group compared with that in the cisplatin group. Among the 335 genes extracted from the DEG analysis and the 100 genes from the GSEA, we selected the 20 overlapping genes as potential candidate genes responsible for the synergistic effects of the combination. The heatmap in Figs. 2B and Supplementary Fig. S4C shows the expression patterns of the candidate genes, revealing that most of these genes exhibited increased expression in response to the treatment. We experimentally validated the function of the candidate genes that have been reported to possess antitumor activity. We knocked down 11 individual genes and observed changes in cell viability in response to individual or combination treatments with cisplatin and narciclasine (Supplementary Fig. S5). Cell viability was reversed on combination treatment when any of the following three genes were silenced: *NOXA*, *MAFF*, and *BTG3* (Fig. 2C). Consistent with the viability results, knockdown of *NOXA*, *MAFF*, and *BTG3* resulted in reduced caspase-7 cleavage (Fig. 2D; Supplementary Fig. S6). We also examined changes in mRNA and protein levels following treatment. The mRNA levels of *NOXA* and *MAFF* increased the most with the combination treatment, which was consistent with the RNA sequencing results, whereas *BTG3* mRNA levels were not (Fig. 2E). Although the protein levels of NOXA, and MAFF were both considerably increased with the combination treatment, the pattern of NOXA expression was more consistent with the results of the previous assays including cell viability, cell death, and apoptosis than that of MAFF (Figs. 1E–I, 2D, F). Additionally, in other NSCLC cell lines, the combination treatment also increased *NOXA* mRNA expression (Supplementary Fig. S7A), and changes in cell viability and apoptosis due to NOXA silencing were consistent with those observed in A549 tumor spheroids (Supplementary Fig. S7B, C). On the basis of these results, NOXA was chosen as the candidate gene underlying the synergistic anticancer effects of the combination of cisplatin and narciclasine.

### NOXA, upregulated by p53, plays a major role in inducing synergistic cell death through regulation of MCL1 in response to the combination treatment of cisplatin and narciclasine

In A549 tumor spheroids, *NOXA* mRNA expression was induced in response to cisplatin alone or in combination with narciclasine (Fig. 2E). Hence, we investigated the effect of the combination treatment on the expression of transcription factors that regulate

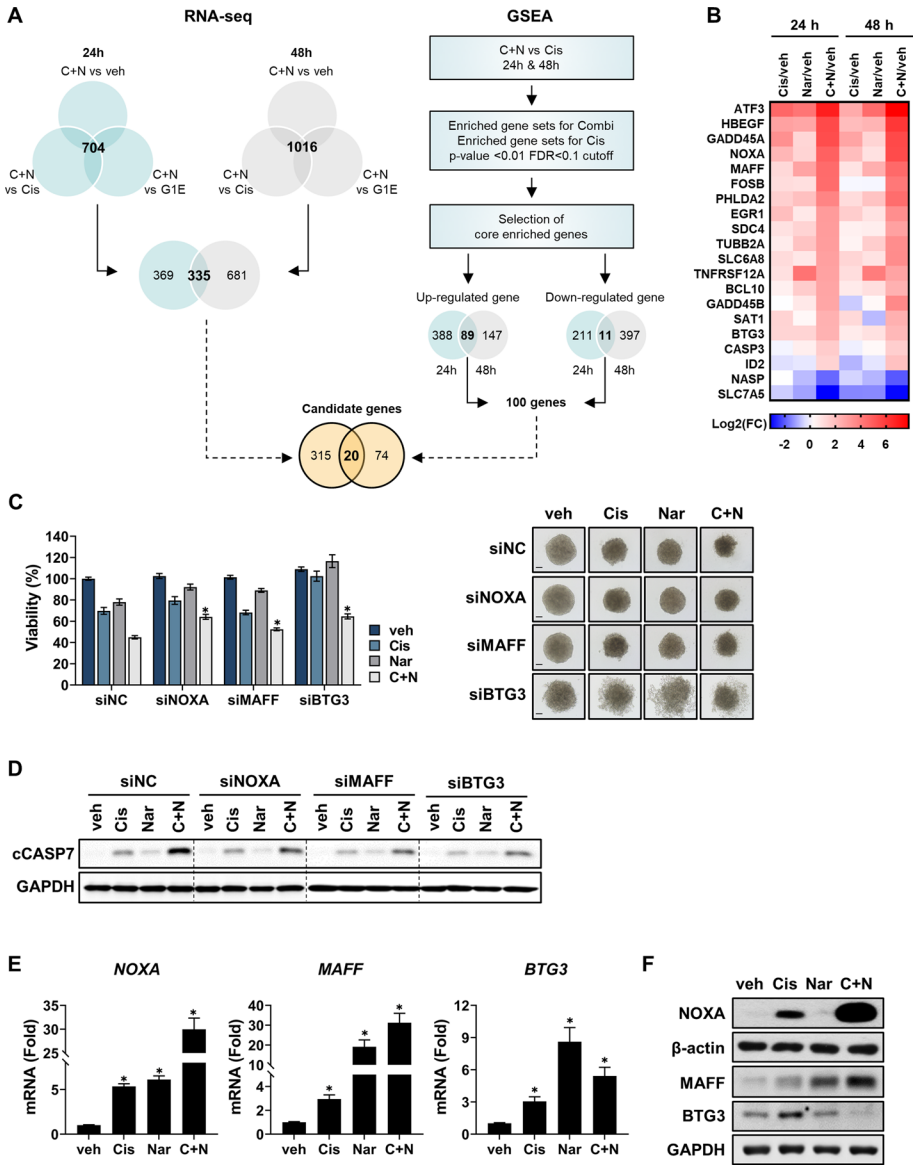


**Fig. 2** NOXA was identified as the candidate gene underlying the synergistic antitumor effects of cisplatin and narciclasine. **A** Schematic overview of the workflow for selection and validation of candidate genes. **B** Heatmap showing the fold changes in the expression of potential candidate genes under different treatment conditions. **C** NOXA-, MAFF-, and BTG3-silenced A549 tumor spheroids were treated with individual or combination treatments of cisplatin and narciclasine for 48 h, and cell viability was assessed by measuring cellular ATP content. *$p < 0.05$ versus combination-treated small interfering RNA for the negative control (siNC). Data are mean ± SEM from three independent experiments in triplicate. Images were taken prior to viability assay. Scale bar: 100 µm. **D** Under the siRNA transfection and treatment conditions described in (**C**), cleaved caspase-7 (cCASP7) levels were analyzed to assess apoptosis. Data represent one of three independent experiments with similar results. **E** Twenty-four hours after treatment of tumor spheroids with individual or combination treatment of cisplatin and narciclasine, the mRNA levels of *NOXA*, *MAFF*, and *BTG3* were assessed using RT-qPCR. Data are presented as fold change in gene expression, normalized to *GAPDH* expression. *$p < 0.05$ versus vehicle. Data are mean ± SEM from three independent experiments in triplicate. **F** Following 48 h of treatment under the indicated treatment conditions, protein levels of NOXA, MAFF, and BTG3 were assessed using western blotting. β-Actin and GAPDH were used as the loading control. Experiments were conducted in triplicate. Data represent one of three independent experiments with similar results

*NOXA* expression. p53 is a well-known upstream regulator of NOXA, and activating transcription factor 3 (ATF3) has been reported to regulate cisplatin-induced NOXA in a p53-independent manner [21, 30]. Considering the dramatic increase in *ATF3* expression after treatment with cisplatin and narciclasine (Fig. 2B; Supplementary Figs. S4C, S7D), we speculated that ATF3 may function as a transcriptional activator of NOXA under these treatment conditions. Hence, we explored whether p53 or ATF3 contributed to the induction of NOXA in response to the combination treatment. To this end, first, the effects of each treatment on the viability of tumor spheroids following transfection with small interfering RNA (siRNA) targeting *TP53* (siTP53) or *ATF3* (siATF3) were examined. When treated with narciclasine alone or in combination with cisplatin, siTP53 tumor spheroids exhibited increased viability compared with those treated with siRNA for the negative control (siNC) (Fig. 3A). Moreover, siTP53-tumor spheroids exhibited a significant decrease in the induction of NOXA in response to the combination treatment at both mRNA and protein levels, which was concomitant with considerably decreased cleavage of caspase-7 (Fig. 3B, C). In contrast, siATF3-tumor spheroids exhibited increased sensitivity to both narciclasine alone and in combination with cisplatin (Fig. 3A). In siATF3-tumor spheroids, the induction of NOXA by the combination treatment was further increased at both the mRNA and protein levels, which was concomitant with an elevation in the cleavage of caspase-7 (Fig. 3B, C). Taken together, these data suggest that NOXA upregulation by the combination treatment is transcriptionally regulated by p53.

NOXA promotes mitochondria-mediated apoptosis by inhibiting anti-apoptotic proteins, including MCL1 [31]. To investigate the effects of increased NOXA induced by the combination treatment on apoptosis-related proteins, we silenced NOXA expression in A549 tumor spheroids and then subjected them to individual or combination treatment with cisplatin and narciclasine. A noticeable difference in the expression of MCL1, a major binding partner of NOXA, was observed in response to the combination treatment (Fig. 3D). MCL1 expression was markedly decreased

(See figure on next page.)

**Fig. 3** NOXA activated the mitochondria-mediated apoptosis pathway in response to the combination treatment by regulating MCL1. **A**, **B** siNC-, siTP53-, or siATF3-transfected A549 tumor spheroids were treated with individual or combination treatments of cisplatin and narciclasine. **A** Cell viability was assessed after treatment for 48 h. *$p < 0.05$ versus vehicle-treated siNC; \$$p < 0.05$ versus narciclasine-treated siNC; †$p < 0.05$ versus combination-treated siNC. Data are mean ± SEM from three independent experiments in triplicate. **B** The levels of the indicated proteins were assessed by western blotting after treatment for 24 h. Vinculin was used as the loading control. Data represent one of three independent experiments with similar results. **C** Twenty-four hours after the indicated treatment, mRNA levels of *NOXA*, *TP53*, and *ATF3* were assessed using RT-qPCR. Data are presented as fold change in gene expression, normalized to *GAPDH* expression. *$p < 0.05$. Data are mean ± SEM from three independent experiments in triplicate. **D**, **E** siNC- or siNOXA-transfected A549 tumor spheroids were treated with individual or combination treatments of cisplatin and narciclasine for 48 h. **D** The expression of intrinsic apoptosis-related proteins was assessed by western blotting. Data represent one of three independent experiments with similar results. **E** Apoptosis was assessed using a cell death detection ELISA kit capable of detecting mono- and oligonucleosomes. *$p < 0.05$. Data are mean ± SD from three independent experiments in triplicate. **F**–**H** A549 tumor spheroids stably transfected with flag-tagged vector control or flag-tagged MCL1 were treated with individual or combination treatments of cisplatin and narciclasine for 48 h. Images were taken prior to viability assay. Scale bar: 100 μm. **F** Cell viability assay, **G** ELISA, and **H** western blotting were performed. *$p < 0.05$. Data in **F** and **G** are mean ± SEM and from three independent experiments in triplicate. Data in **H** represent one of three independent experiments with similar results

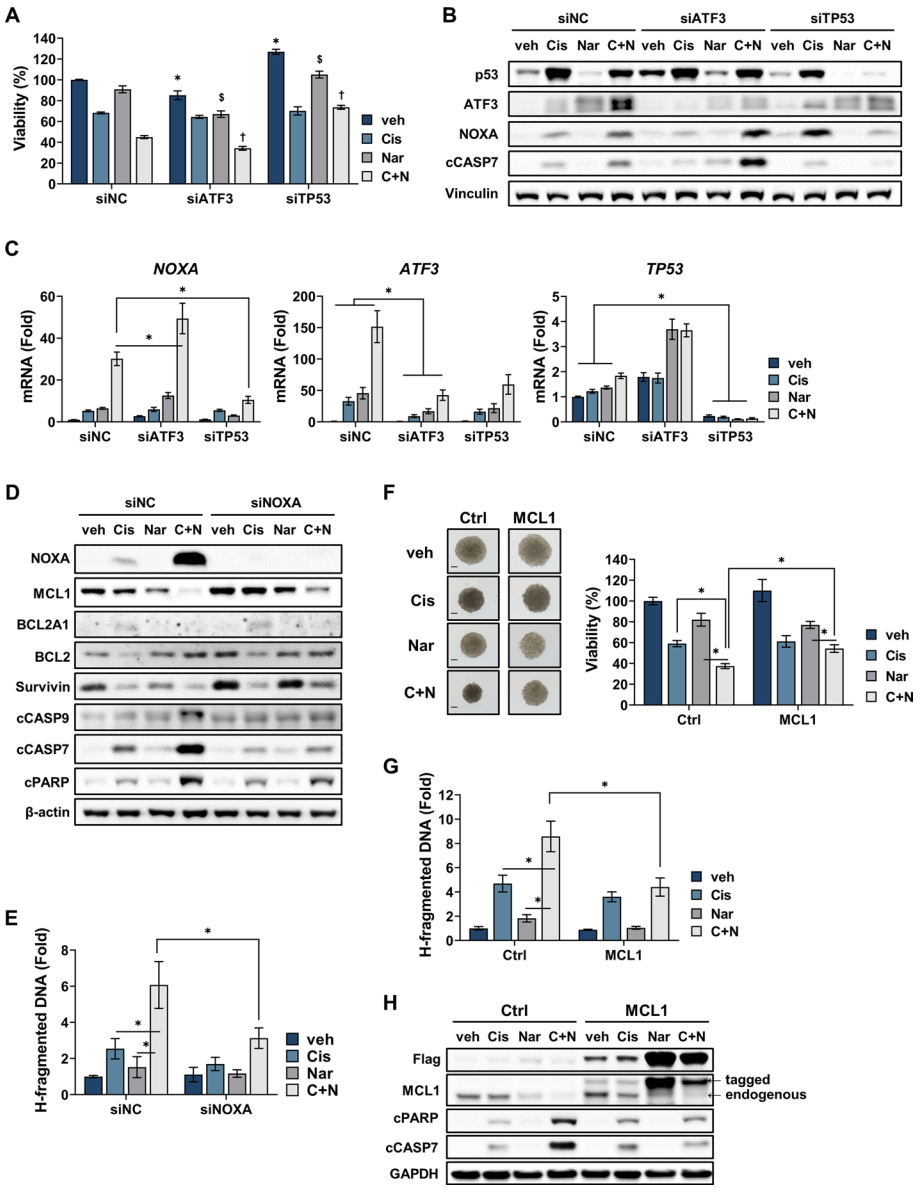


**Fig. 3** (See legend on previous page.)

with the combination treatment when compared with cisplatin or narciclasine alone. Following NOXA knockdown, the basal expression of MCL1 increased marginally, and the decrease in MCL1 expression induced by the combination treatment was also reversed. On the other hand, BCL2A1 expression was almost undetectable irrespective of the treatment, except that it increased slightly in cisplatin-treated tumor spheroids. Consistently, combination treatment alongside NOXA knockdown had minimal effects on BCL2 expression. Survivin, a member of the inhibitor of apoptosis protein family, expression was downregulated by cisplatin and the combination treatment, and this was reversed by NOXA knockdown. The decrease in survivin protein levels, encoded by the *BIRC5* gene, induced by cisplatin and the combination treatment were a result of decreased mRNA expression (Supplementary

Fig. S8C). The increased cleavage of caspase-9, the downstream effector caspase-7, and the caspase substrate poly (ADP-ribose) polymerase (PARP) induced by the combination treatment was considerably reduced following NOXA knockdown (Fig. 3D). Consistent with these observations, a cell death assay that quantifies histone-associated DNA fragmentation showed that NOXA knockdown significantly inhibited cell death induced by the combination treatment (Fig. 3E). These findings suggest that the combination treatment induced apoptosis via NOXA-induced downregulation of MCL1.

The enhanced viability observed upon NOXA knockdown was significantly diminished in tumor spheroids in which both NOXA and MCL1 were concurrently silenced (Supplementary Fig. S8A). Consistent with these observations, the results of the cell death assay also demonstrated that the concurrent silencing of NOXA and MCL1 significantly enhanced apoptosis induced by the combination treatment when compared with silencing of NOXA alone (Supplementary Fig. S8B). Because survivin expression was consistent with combination treatment-induced apoptosis, we further verified the role of survivin. Although the effect of survivin knockdown appeared to be similar to that of MCL1, reversal of combination treatment-induced apoptosis was more pronounced with MCL1 knockdown (Supplementary Fig. S8D, E). To further confirm that MCL1 plays a pivotal role in combination treatment-induced apoptosis, we utilized MCL1-overexpressing A549 cells. In MCL1-overexpressing tumor spheroids, the significant decrease in viability induced by combination treatment was notably reversed (Fig. 3F). The results of the cell death assay and cleavage of PARP and caspase-7 also confirmed that MCL1-overexpressing tumor spheroids exhibited a reduction combination treatment-induced apoptosis (Fig. 3G, H). Taken together, these results suggest that NOXA plays a major role in the observed synergistic effects of the combination of cisplatin and narciclasine, and that NOXA-mediated regulation of MCL1 levels underlies the induction of apoptosis in response to the combination treatment in NSCLC tumor spheroids.

### Narciclasine both alone and in combination with cisplatin downregulates MCL1 expression through inhibition of translation

Interestingly, although narciclasine decreased MCL1 protein levels (Fig. 3D), its mRNA levels were significantly upregulated shortly after the treatment (Fig. 4A). To clarify whether narciclasine-induced decrease in MCL1 levels was potentially due to accelerated proteasomal degradation, A549 cells were treated with narciclasine and MG-132, a proteasomal inhibitor. MG-132 treatment alone induced a time-dependent accumulation of MCL1 protein (Fig. 4B). However, despite the inhibition of protein degradation by MG-132 treatment, accumulation of MCL1 was not observed in narciclasine-treated cells (Fig. 4B). Despite the elevated mRNA levels in response to narciclasine treatment, the absence of an increase in MCL1 protein levels and the acceleration of protein degradation suggests that translation of MCL1 is inhibited. The kinetics of the decrease in MCL1 expression by narciclasine were similar to those of cycloheximide, a widely used translation inhibitor, confirming that narciclasine inhibited the translation of *MCL1* mRNA (Fig. 4C). To confirm the effect of narciclasine on protein translation, a surface sensing of translation (SUnSET) assay was used to assess

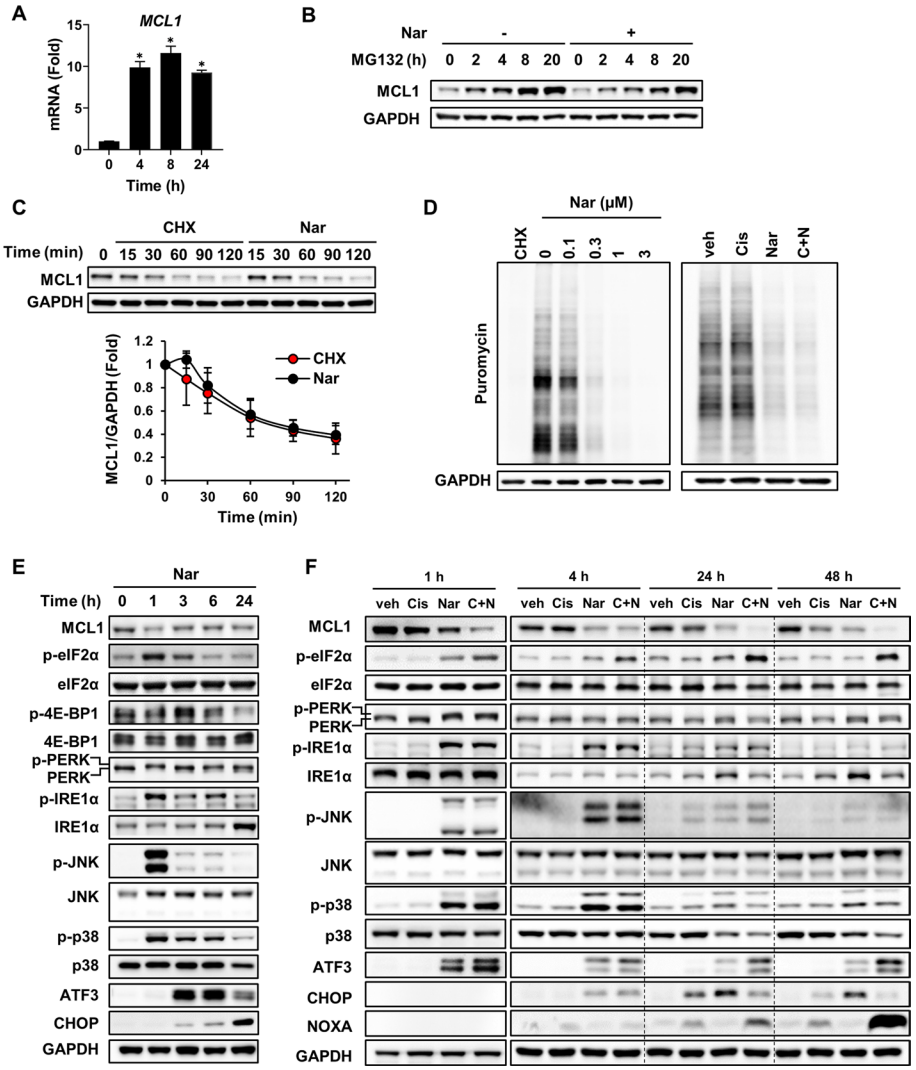


**Fig. 4** Narciclasine and the combination treatment reduced MCL1 levels through inhibition of translation. **A** A549 tumor spheroids were treated with 0.3 μM narciclasine for the indicated time periods, and *MCL1* mRNA levels were quantified using RT-qPCR. Data are presented as fold change in *MCL1* expression, normalized to *GAPDH* expression. *$p < 0.05$. Data are mean ± SEM from three independent experiments in triplicate. **B** A549 tumor spheroids were pretreated with 0.3 μM narciclasine for 2 h before treatment with 10 μM MG-132 for the indicated time periods. MCL1 protein levels were analyzed by western blotting. Data represent one of three independent experiments with similar results. **C** A549 tumor spheroids were treated with 10 μg/mL cycloheximide and 0.3 μM narciclasine for the indicated time periods. Data are mean ± SD from three independent experiments. **D** Protein synthesis was assessed using surface sensing of translation assay. A549 tumor spheroids were treated as indicated doses of narciclasine for 2 h, followed by incubation with 5 μg/mL puromycin for 15 min. For the right panel, cisplatin and narciclasine were treated at concentrations of 10 and 0.3 μM, respectively. Whole cell lysates were obtained and subjected to western blotting using anti-puromycin antibody. Data represent one of three independent experiments with similar results. **E** A549 tumor spheroids were treated with 0.3 μM narciclasine for the indicated time periods. Levels of phospho-eIF2α, phospho-4E-BP1, and other proteins involved in the unfolded protein response (UPR) pathway were analyzed by western blotting. Data represent one of three independent experiments with similar results. **F** Whole cell lysates were prepared from A549 tumor spheroids treated with 10 μM cisplatin, 0.3 μM narciclasine, or the combination for the indicated time. Levels of proteins involved in the UPR pathway were analyzed by western blotting. Data represent one of three independent experiments with similar results

protein synthesis in A549 tumor spheroids. Narciclasine was found to reduce the levels of nascent peptides in a dose-dependent manner (Fig. 4D). Although cisplatin alone did not decrease protein synthesis, the combination of cisplatin and narciclasine resulted in a dramatic inhibition of translation, similar to that observed with narciclasine alone (Fig. 4D).

Subsequently, we examined the effect of narciclasine and the combination treatment on pathways that regulate protein translation, including the mTOR and integrated stress response (ISR) pathways [32, 33]. Narciclasine promptly increased the phosphorylation of eIF2α, a key factor in ISR including a reduction of general protein synthesis, which may explain the observed rapid decrease in MCL1 levels (Fig. 4E). However, the phosphorylation of 4E-BP, a target protein in the mTOR pathway, was only modestly increased at later time points (Fig. 4E). Protein kinase R-like endoplasmic reticulum kinase (PERK), one of the eIF2α kinases, responds to endoplasmic reticulum (ER) stress and activates unfolded protein response (UPR) [33]. PERK phosphorylation increased promptly after narciclasine treatment, consistent with eIF2α phosphorylation, indicating that PERK was the upstream kinase (Fig. 4E). Furthermore, narciclasine markedly elevated the phosphorylation of another ER stress sensor, inositol-requiring enzyme type 1α (IRE1α), resulting in increased phosphorylation of its downstream targets c-Jun N-terminal kinase (JNK) and p38 [34, 35]. The expression of ATF3 and C/EBP homologous protein (CHOP), which are transcription factors induced by ER stress [36], was also increased following narciclasine treatment (Fig. 4E).

Next, we examined the expression of UPR signaling-associated proteins at 1, 4, 24, and 48 h following cisplatin, narciclasine, or the combination treatment (Fig. 4F). eIF2α phosphorylation was higher with the combination treatment than that with narciclasine alone, and this elevation was sustained for up to 48 h. PERK and IRE1α phosphorylation levels were increased in cells treated with narciclasine and the combination treatment. ATF3 exhibited the most notable upregulation in tumor spheroids subjected to the combination treatment, whereas CHOP expression was the highest with narciclasine treatment. In general, changes in expression of proteins involved in the UPR were minimal with cisplatin treatment (Fig. 4F).

The accumulation of misfolded proteins resulting from excessive ROS generated by intrinsic and extrinsic pathways leads to UPR [37–39]. Treatment with narciclasine significantly increased $H_2O_2$ levels, which is postulated to be a potential inducer for ER stress (Supplementary Fig. S9). Notably, combination treatment of cisplatin and narciclasine resulted in a greater increase in $H_2O_2$ levels than those observed with either compound alone (Supplementary Fig. S9).

Taken together, these results suggest that enhanced ROS production following treatment with narciclasine both alone and in combination with cisplatin activated ER stress-induced UPR via PERK and IRE1α pathway, leading to the translational inhibition of MCL1.

#### NOXA regulation in response to ROS generated by combination treatment with cisplatin and narciclasine is mediated via the IRE1α–JNK/p38 axis

The expression of NOXA was significantly increased following combination treatment of cisplatin and narciclasine (Fig. 2E, F). In addition to the previously mentioned p53

as a regulator of NOXA (Fig. 3B, C), to further elucidate the mechanisms underlying NOXA upregulation in response to the combination treatment, we investigated the potential involvement of ER stress-induced UPR pathways, via PERK and IRE1α. We pretreated tumor spheroids with either GSK2606414, a PERK inhibitor, or KIRA6, an IRE1α inhibitor, prior to combination treatment, and subsequently analyzed *NOXA* mRNA levels. Pretreatment with the PERK inhibitor failed to suppress the combination treatment-induced increase in *NOXA* expression (Fig. 5A). However, IRE1α inhibition by KIRA6 pretreatment significantly inhibited *NOXA* mRNA expression at 4 h and 24 h post-treatment with cisplatin and narciclasine (Fig. 5B). Consistent with the mRNA results, the combination treatment-induced NOXA protein was markedly suppressed when kinase activity of IRE1α was inhibited (Fig. 5C). Moreover, the increase in CHOP and ATF3 levels was also attenuated by IRE1α inhibition (Fig. 5C). These results indicate that the combination treatment-induced upregulation of NOXA is primarily mediated through IRE1α-driven UPR processes, rather than the PERK pathway.

When IRE1α is activated, it recruits TNF receptor-associated factor 2 (TRAF2), which subsequently activates apoptosis signal-regulating kinase 1 (ASK1), an upstream kinase that phosphorylates and activates both JNK and p38 pathways [40–42]. Previous report also showed that NOXA expression was enhanced through IRE1α–JNK signaling pathways [43]. Pretreatment with KIRA6 effectively blocked the phosphorylation of p38 induced by narciclasine or the combination treatment, while JNK phosphorylation was only slightly inhibited (Fig. 5C). Next, we inhibited JNK and p38 activities using pharmacological inhibitors and subsequently analyzed changes in *NOXA* mRNA and protein levels following the combination treatment. Treatment with SP600125, a JNK inhibitor, attenuated the narciclasine- and combination-induced phosphorylation of JNK. Treatment with SB203580, a p38 inhibitor, reduced the phosphorylation of serine 727 of STAT1, a downstream target of p38 (Fig. 5E), consistent with previous reports [44, 45]. As expected, inhibition of p38 led to substantial reductions in both NOXA mRNA and protein levels in tumor spheroids exposed to the combination treatment, suggesting

(See figure on next page.)

**Fig. 5** NOXA regulation in response to ROS generated by combination treatment with cisplatin and narciclasine is mediated via the IRE1α–JNK/p38 axis. A549 tumor spheroids were pretreated with **A** 50 nM of GSK414, a PERK inhibitor, or **B** 100 nM of KIRA6, an IRE1α inhibitor, for 1 h, followed by treatment with 10 μM cisplatin, 0.3 μM narciclasine, or their combination for 4 or 24 h. *NOXA* mRNA levels were evaluated using RT-qPCR. Data are presented as fold change of *NOXA* expression, normalized to GAPDH expression. †$p < 0.05$ versus narciclasine; *$p < 0.05$ versus combination. Data are mean ± SEM from three independent experiments in triplicate. **C** Under the treatment condition described in **A** and **B**, levels of proteins involved in the UPR pathway were analyzed by western blotting. Data represent one of three independent experiments with similar results. **D** A549 tumor spheroids were pretreated with 10 μM of SP600125, a JNK inhibitor or SB203580, a p38 inhibitor for 1 h, followed by treatment with 10 μM cisplatin, 0.3 μM narciclasine, or their combination for 4 h or 24 h. NOXA mRNA levels were evaluated using RT-qPCR. Data are presented as fold change in *NOXA* expression, normalized to GAPDH expression. †$p < 0.05$ versus narciclasine; *$p < 0.05$ versus combination. Data are mean ± SEM from three independent experiments in triplicate. **E** Under the treatment condition described in **D**, levels of proteins involved in UPR pathway were analyzed by western blotting. Data represent one of three independent experiments with similar results. **F** A549 tumor spheroids were pretreated with 10 mM NAC (*N*-acetylcysteine) or 0.5 mM glutathione ethyl ester (GSH-EE) for 1 h, followed by treatment with 10 μM cisplatin, 0.3 μM narciclasine, or their combination for 1 or 24 h. Levels of proteins involved in the UPR pathway were analyzed by western blotting. Data represent one of three independent experiments with similar results

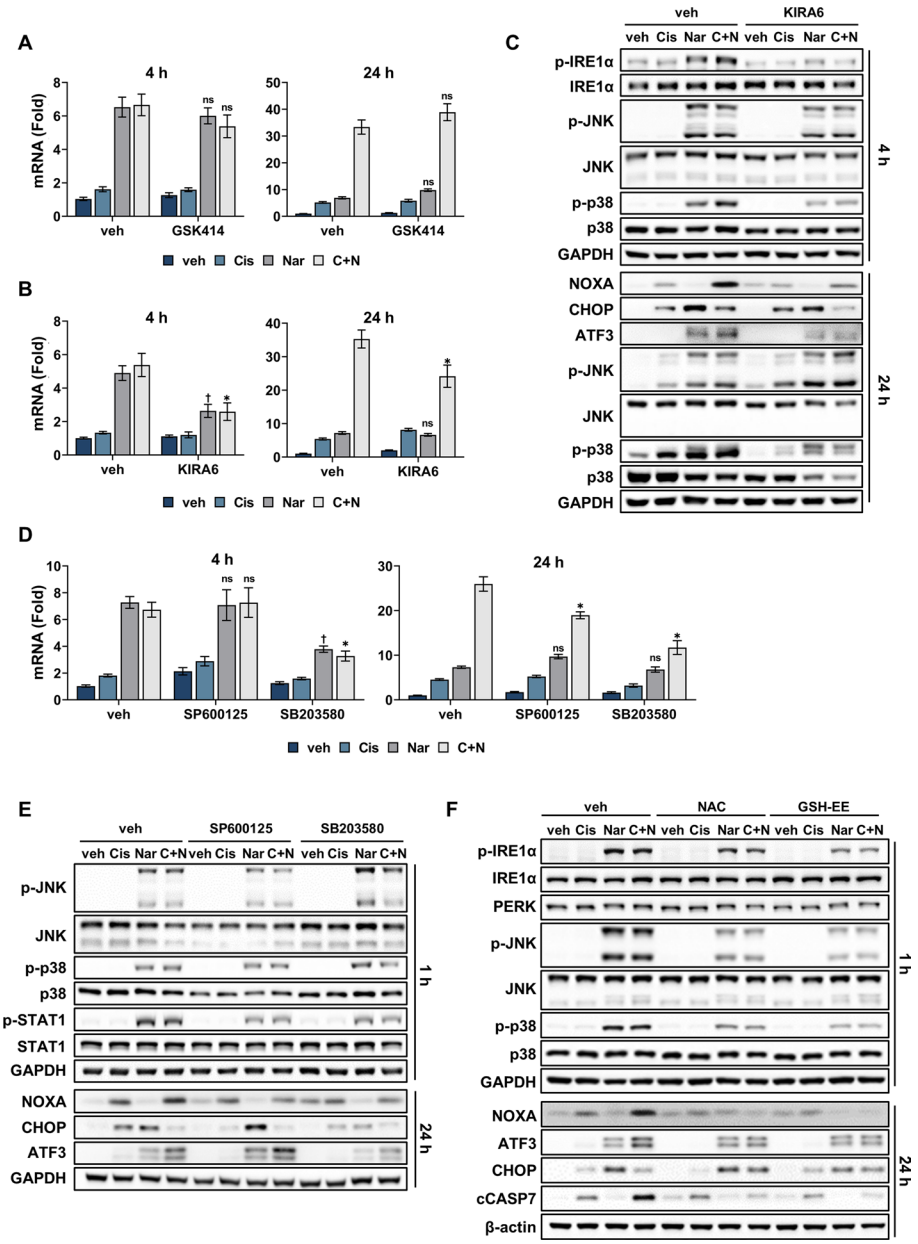


**Fig. 5** (See legend on previous page.)

the critical role of p38 in NOXA regulation (Fig. 5D, E). Interestingly, JNK inhibition lowered *NOXA* mRNA levels by only 18%, but it reduced NOXA protein to a level comparable to that observed with p38 inhibition, indicating that JNK primarily regulates the levels of NOXA protein (Fig. 5D, E). In addition, ATF3 induction by combination treatment was associated with IRE1α–p38 signaling (Fig. 5C, E). Collectively, these results suggest that the IRE1α–JNK/p38 axis contributes to the upregulation of NOXA in response to the combination treatment.

To determine whether ROS activates the IRE1α–JNK/p38 pathway and facilitates NOXA induction, we conducted experiments using the antioxidants *N*-acetylcysteine (NAC) and glutathione ethyl ester (GSH-EE). Cells were pretreated with NAC (10 mM)

or GSH-EE (0.5 mM) for 1 h before cisplatin, narciclasine, or combination treatment. Western blot analysis revealed that IRE1α, JNK, and p38 phosphorylation levels were partially reduced upon antioxidant pretreatment, but not PERK, indicating that ROS induced by narciclasine or combination treatment contributes to the activation of the IRE1α–JNK/p38 pathway. Furthermore, the combination treatment-induced upregulation of NOXA and cleaved caspase-7 was abolished in the presence of antioxidants (Fig. 5F). These results indicate that ROS induced by the combination treatment enhances NOXA expression and apoptosis by activating the IRE1α–JNK/p38 pathway.

### Cisplatin, both alone and in combination with narciclasine, promotes NOXA-mediated MCL1 degradation

Despite the increased *MCL1* mRNA expression and proficient translation in response to cisplatin treatment (Figs. 4D, 6A), its protein levels were decreased when compared with that in vehicle-treated cells (Figs. 3D, 4F), suggesting that MCL1 protein levels are regulated by a post-translational mechanism. Therefore, we pretreated A549 tumor spheroids with MG-132 prior to individual or combination treatments with cisplatin and narciclasine and assessed MCL1 levels by western blotting. MG-132 pretreatment increased basal levels of MCL1 and further induced accumulation of MCL1 in response to cisplatin treatment (Fig. 6B). This suggests that cisplatin induces proteasomal degradation of MCL1, which is consistent with previous reports [27]. However, following MG-132 pretreatment, tumor spheroids treated with narciclasine exhibited lower levels of MCL1 than those treated with the vehicle, confirming that narciclasine inhibited the translation of MCL1, as shown in Fig. 4. The decrease in MCL1 protein levels induced by the combination treatment were not restored with MG-132 pretreatment to the same degree as that seen with narciclasine (Fig. 6B). This could be due to the fact that *MCL1* mRNA levels were much lower in the combination treatment group than that in the narciclasine group, and protein synthesis may have also been lower. At 48 h, MCL1 levels were lower by 4.2-fold in the combination group than in the narciclasine group. With MG-132 pretreatment, the decrease was only 1.6-fold when compared with narciclasine alone, indicating increased proteasomal degradation of MCL1 with the combination treatment when compared with narciclasine alone.

Our data suggest that NOXA, which increased in response to cisplatin alone or in combination with narciclasine, plays an important role in MCL1 degradation (Figs. 3D, 6B). Hence, we analyzed changes in MCL1 levels using cycloheximide chase assay following each treatment, with or without knockdown of *NOXA* (Fig. 6C). The half-life of MCL1 in the untreated group was about 41.8 min and considerably shorter in the group treated with cisplatin ($t_{1/2} = 30.3 \pm 1.9$ min). The half-life of MCL1 in the combination of cisplatin and narciclasine ($t_{1/2} = 24.9 \pm 1.4$ min) was the shortest, likely owing to the highest induction of NOXA (Fig. 6D). Additionally, NOXA knockdown extended the half-lives of MCL1 in the vehicle- ($t_{1/2} = 51.1 \pm 4.4$ min), cisplatin- ($t_{1/2} = 47.9 \pm 7.4$ min), and combination-treated ($t_{1/2} = 49.1 \pm 6.2$ min) groups (Fig. 6D). The stability of MCL1 was enhanced when NOXA was silenced, which confirms that the increase in NOXA levels in response to cisplatin and the combination treatment mediated the degradation of MCL1.

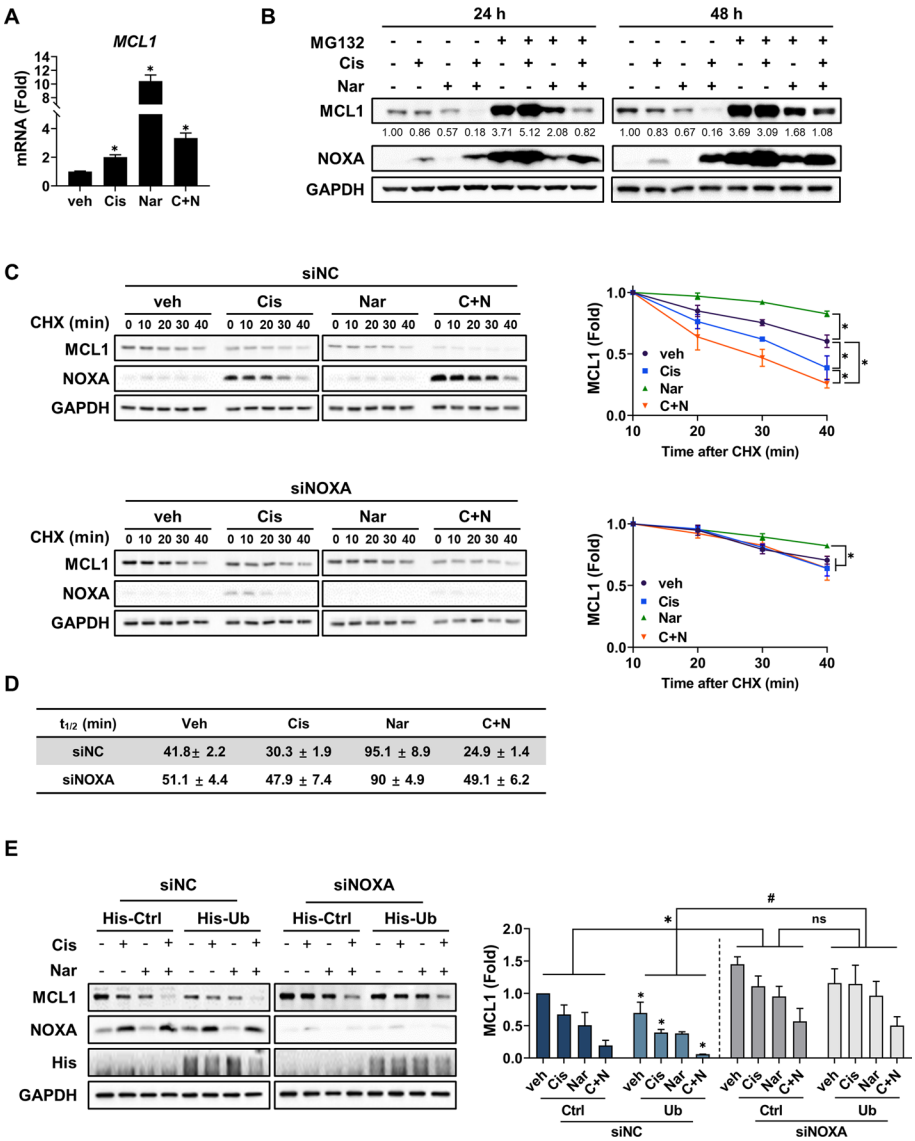


| $t_{1/2}$ (min) | Veh | Cis | Nar | C+N |
|---|---|---|---|---|
| siNC | 41.8± 2.2 | 30.3 ± 1.9 | 95.1 ± 8.9 | 24.9 ± 1.4 |
| siNOXA | 51.1 ± 4.4 | 47.9 ± 7.4 | 90 ± 4.9 | 49.1 ± 6.2 |

**Fig. 6** NOXA induced by cisplatin and the combination treatment augmented MCL1 degradation. **A** Twenty-four hours after treatment of A549 tumor spheroids with individual or combination treatments of cisplatin and narciclasine, *MCL1* mRNA levels were evaluated using RT-qPCR. Data are presented as fold change in *MCL1* expression, normalized to *GAPDH* expression. *$p < 0.05$. Data are mean ± SEM from three independent experiments in triplicate. **B** A549 tumor spheroids were pretreated with 10 μM MG-132 for 1 h, followed by treatment with 10 μM cisplatin, 0.3 μM narciclasine, or their combination for 24 and 48 h. MCL1 and NOXA levels were analyzed by western blotting. Numbers below the blot represent relative levels of the proteins, normalized to GAPDH levels. Data represent one of three independent experiments with similar results. **C** A549 cells transfected with siNC or siNOXA were pretreated with 5 μM cisplatin, 0.1 μM narciclasine, or their combination for 24 h before treatment with 10 μg/mL cycloheximide (CHX) for the indicated time periods. MCL1 and NOXA levels were measured by western blotting. MCL1 levels were quantified and normalized to GAPDH as shown in the right panel. *$p < 0.05$. Data are mean ± SD from three independent experiments. **D** Half-life $t_{1/2}$ of MCL1 was calculated using linear regression analysis on the graph (**C**). **E** A549 cells were co-transfected with the siNC or siNOXA with or without transfection of His-tagged ubiquitin (His-Ub) for 24 h, followed by the indicated treatment for 24 h. MCL1 and NOXA levels in the whole cell lysates were measured by western blotting. MCL1 levels were quantified and normalized to GAPDH as shown in the right panel. *$p < 0.05$ versus same treatment group with His-Ctrl and siNC, #$p < 0.05$ versus same treatment group with His-Ub and siNC. Data are mean ± SD from three independent experiments

To investigate whether NOXA-mediated MCL1 degradation occurred through the ubiquitin–proteasome pathway, A549 cells were co-transfected with siNC or siNOXA, and a polyhistidine-tagged control (His-Ctrl) or ubiquitin (His-Ub), followed by treatment with cisplatin, narciclasine, or their combination (Fig. 6E). MCL1 levels were lower following His-Ub transfection compared with that with His-Ctrl transfection in the vehicle-, cisplatin-, and combination-treated groups. Consistent with our expectations, there was an overall increase in MCL1 levels in cells transfected with siNOXA compared with those transfected with siNC. However, in the absence of NOXA, MCL1 levels did not change significantly with the forced expression of ubiquitin (His-Ub), suggesting that NOXA is required for the ubiquitination of MCL1 (Fig. 6E). Specifically, with the combination treatment and forced expression of ubiquitin, MCL1 levels decreased to 25% compared with the combination-treated His-Ctrl group; however, in the NOXA knockdown groups, MCL1 levels were similar, irrespective of the ubiquitin levels. In other words, the combination treatment significantly induced NOXA expression, which mediated the ubiquitin-proteasomal degradation of MCL1.

Taken together, our results indicated that the combination of cisplatin and narciclasine significantly increased NOXA expression, which downregulated MCL1 by enhancing proteasomal degradation, as well as inducing translational inhibition of MCL1, ultimately resulting in synergistic apoptotic cell death in NSCLC tumor spheroids.

## Discussion

We utilized a three-dimensional (3D) culture system, which has been shown to be a more physiologically relevant model than conventional two-dimensional (2D) cultures, to identify a compound for combination therapy with cisplatin. Tumor spheroids as a 3D in vitro tumor model reproduce aspects of the tumor microenvironment observed in solid tumors, including cell–cell and cell–matrix interactions, as well as nutrient and oxygen gradients [46]. These factors also affect drug penetration and diffusion, providing a better prediction of in vivo drug response [46]. The usefulness of tumor spheroids has been highlighted in cancer research, including for the characterization of tumor growth and development, cancer target discovery, and cancer drug screening [47]. In the present study, consistent with previous studies, tumor spheroids exhibited reduced sensitivity to drugs compared with cells cultured in 2D (Supplementary Table S1) [48–50].

In this work, we identified a natural product, narciclasine, that sensitizes NSCLC cells to cisplatin, suggesting a potential combination treatment for NSCLC resistant to current standard treatments. We aimed to elucidate the cellular mechanisms underlying the synergistic anticancer effects of cisplatin and narciclasine. Our results showed that concurrent treatment with cisplatin and narciclasine significantly reduced cell viability and induced apoptosis, thereby enhancing the sensitivity of cisplatin-resistant NSCLC tumor spheroids to cisplatin. Mechanistically, cisplatin induced NOXA expression, facilitating the proteasome-dependent degradation of MCL1, whereas narciclasine inhibited *MCL1* translation by activating the UPR. Therefore, these compounds function via distinct mechanisms to downregulate the expression of MCL1, resulting in potentiated synergistic anticancer activity.

Synergistic effects of the combination were observed in NSCLC tumor spheroids derived from four cell lines with different genetic backgrounds: A549 ($KRAS^{G12S}$),

NCI-H358 (*KRAS*$^{G12C}$ and *TP53*$^{null}$), HCC2279 (*EGFR*$^{\Delta746-\Delta750}$ and *TP53*$^{Y234C}$), and NCI-H1975 (*EGFR*$^{L858R/T790M}$ and *TP53*$^{R237H}$) (Supplementary Fig. S2) [51]. This suggests that the proposed combination approach is broadly applicable to refractory cancers, including EGFR-TKI-resistant cancers, irrespective of their genetic background.

The expression of NOXA, a target gene of p53, increases in response to DNA damage [21], consistent with our results (Fig. 3A–C). NOXA can also be induced by various other transcription factors, such as ATF3/ATF4, HIF1α, p73, and KLF4, in response to various cellular stresses [31, 52–55]. Herein, we observed the induction of *NOXA* mRNA expression in NCI-H1975, NCI-H358, and HCC2279 tumor spheroids, in which p53 functionality was impaired (Supplementary Fig. S7A). These results suggest that NOXA can be induced through a p53-independent mechanism in cells with defective p53 expression.

*ATF3* was one of the most inducible genes following the combination treatment in all four NSCLC tumor spheroids (Fig. 2B; Supplementary Figs. S4C, S7D). ATF3 functions as both a pro- and anti-tumorigenic molecule, depending on the cellular context and tumor type [56]. ATF3 binds directly to p53 protein, preventing ubiquitin-mediated degradation of p53, and thereby increasing its function in response to DNA damage [57]. In contrast, knockdown of ATF3 in lung cancer cell lines has been reported to inhibit cell proliferation, migration, and invasion [58]. In this study, knockdown of ATF3 resulted in decreased cell viability and enhanced cell death, possibly via de-repression of NOXA (Fig. 3A–C), suggesting that ATF3 may function as a survival factor. Under combination treatment conditions, ATF3 was induced along with NOXA (Fig. 4F). However, the onset of increases in NOXA and ATF3 protein levels occurred at different times after combination treatment. ATF3 was rapidly induced 1 h after treatment (Fig. 4F), whereas NOXA increase was not observed until 24 h after treatment. These results suggest that, during the early phase after treatment, NOXA expression may be suppressed by ATF3, whereas it is activated by ROS-activated IRE1α–JNK/p38 signaling, resulting in only modest induction of NOXA within 24 h of combination treatment (Figs. 3C, 4F, 5B, D, F). Then, p53 accumulation became evident 24 h after treatment (Supplementary Fig. S10), and accordingly, an increase in NOXA expression was stronger and sustained in the later time points (Fig. 4F). In other words, temporal changes in the strength of multiple regulatory signaling pathways, p53, ROS-activated IRE1α–JNK/p38, and IRE1α–p38–ATF3 led to the dominant upregulation of NOXA, which may counteract the survival effect of ATF3, ultimately shifting the balance toward apoptotic cell death. A similar phenomenon has been observed in TNF-α signaling, which can paradoxically promote either cell survival or death depending on the balance of competing signals. TNF-α activates NF-κB, promoting the expression of pro-survival genes, while simultaneously activating caspase-8 via the TNF receptor-associated death domain, leading to apoptosis [59]. The final outcome regarding whether the cell survives or undergoes apoptosis is determined by the relative strength of these opposing signals.

In A549, NCI-H1975, and HCC2279 tumor spheroids, NOXA protein expression was elevated following combination treatment (Fig. 2F; Supplementary Fig. S7C). In NCI-H358 tumor spheroids, despite similar mRNA levels, NOXA protein levels increased with combination treatment when compared with narciclasine alone, which mediated the inhibition of translation (Supplementary Fig. S7A, C), suggesting the stabilization

of NOXA by the combination treatment. NOXA is post-translationally regulated by the E3 ubiquitin ligase carboxy-terminus of hsc70 interacting protein and deubiquitinase ubiquitin carboxy-terminal hydrolase-L1 [60, 61]. Further, NOXA is stabilized upon exposure to hydrogen peroxide owing to the inhibition of proteasomal degradation [62]. This may explain why NOXA levels with the combination treatment were lower than those with control or cisplatin treatment in the presence of MG132 in A549 tumor spheroids (Fig. 6B).

NOXA is induced by various anticancer agents, including cisplatin, paclitaxel, and bortezomib, which promote apoptotic cell death via mechanisms such as transcriptional regulation and protein stabilization [31]. In response to cellular stress, NOXA levels are elevated, and it preferentially binds to MCL1 and promotes its ubiquitin-mediated proteasomal degradation, thereby decreasing the half-life of MCL1 [63, 64]. Consistent with previous reports, the half-life of MCL1 was notably reduced by the combination treatment, in which NOXA expression was the highest (Fig. 6C). MCL1 stability is regulated by various E3 ubiquitin ligases and deubiquitinases [65]. On the basis of RNA sequencing results, we noted that the mRNA levels of ubiquitin-specific protease 13 (*USP13*), the deubiquitinase responsible for removing polyubiquitin chains from MCL1 [66], was decreased approximately 4- to 15-fold following combination treatment in all four NSCLC tumor spheroids (Supplementary Fig. S8F). This decline in USP13 expression may also contribute to the complete downregulation of MCL1 by the combination treatment, alongside NOXA-mediated MCL1 degradation.

The cytotoxicity of narciclasine was evaluated against 60 human cancer cell lines by the National Cancer Institute, and the mean 50% growth inhibition ($GI_{50}$) was 16 nM, demonstrating its potent anticancer activity [67, 68]. In contrast to cancer cells, normal cells are less sensitive to narciclasine [16, 17]. Although various mechanisms have been reported to underlie the anticancer effects of narciclasine, the relationship between narciclasine and ER stress has not yet been explored. In the present study, we report that narciclasine activated the ER stress sensors PERK and IRE1α and their downstream targets eIF2α, JNK, and p38 mitogen-activated protein kinase, respectively (Fig. 4E). These signaling pathways ultimately converge upon the induction of CHOP [69], whose levels were elevated after treatment with narciclasine (Fig. 4E, F). In addition to the previously reported function of narciclasine with respect to suppressing protein translation through binding to eEF1A [19], we found that narciclasine inhibited protein translation via phosphorylation of eIF2α, a critical factor in stress-mediated translation inhibition (Fig. 4D, E). Therefore, our findings demonstrated that narciclasine triggered UPR response through activation of the PERK–eIF2α and IRE1α–JNK/p38 axes.

In addition to our findings that NOXA upregulation induced by the combination treatment is regulated by p53, we further discovered that NOXA expression is controlled by the UPR through the IRE1α–JNK/p38 axis. Various stressors such as TNF-α, lipopolysaccharide (LPS), and ultraviolet (UV) irradiation trigger p38-mediated phosphorylation of STAT1 at the Ser727 residue [44]. Phosphorylation of STAT1 at S727 enhances transcriptional activity of p53, resulting in increased induction of pro-apoptotic genes including *NOXA*, *BAX*, and *Fas* [70]. This suggests that the dramatic elevation in NOXA expression induced by the combination treatment is possibly due to p53 stimulation through distinct cellular signaling.

## Conclusions

We demonstrated that narciclasine sensitized cisplatin-resistant NSCLC tumor spheroids to cisplatin by inducing apoptosis. Mechanistically, combination treatment with narciclasine and cisplatin attenuated MCL1 through translation inhibition, and induced NOXA, which further facilitated MCL1 degradation. Thus, the combination of cisplatin and narciclasine presents a promising therapeutic strategy that can overcome chemoresistance and potentially improve treatment outcomes.

**Abbreviations**

| | |
|---|---|
| ATF3 | Activating transcription factor 3 |
| BCL2 | B-cell lymphoma 2 |
| BCL2A1 | B-cell lymphoma 2-related protein A1 |
| BH3 | Bcl-2 homology 3 |
| CHOP | C/EBP homologous protein |
| DEG | Differentially expressed gene |
| eEF1A | Eukaryotic elongation factor 1-alpha |
| ER | Endoplasmic reticulum |
| GSEA | Gene set enrichment analysis |
| IRE1α | Inositol-requiring enzyme type 1α |
| JNK | C-Jun N-terminal kinase |
| MCL1 | Myeloid cell leukemia-1 |
| mTOR | Mammalian target of rapamycin |
| NSCLC | Non-small cell lung cancer |
| PERK | Protein kinase R-like endoplasmic reticulum kinase |
| PMAIP1 | Phorbol-12-myristate-13-acetate-induced protein 1 |
| ROS | Reactive oxygen species |
| STAT3 | Signal transducer and activator of transcription 3 |
| UPR | Unfolded protein response |

## Supplementary Information

The online version contains supplementary material available at https://doi.org/10.1186/s11658-025-00735-5.

Additional file 1: Supplementary Table 1. Comparison of $IC_{50}$ values of cisplatin and narciclasine in 2D and 3D cell culture systems. Supplementary Fig. 1. Cisplatin and narciclasine inhibited the viability of NSCLC tumor spheroids. Supplementary Fig. 2. Narciclasine significantly enhanced cisplatin sensitivity in cisplatin-resistant NSCLC tumor spheroids. Supplementary Fig. 3. Apoptosis analysis by flow cytometry. Supplementary Fig. 4. Differentially expressed genes (DEGs) and gene set enrichment analyses (GSEA) in A549 tumor spheroids. Supplementary Fig. 5. Functional validation of candidate genes. Supplementary Fig. 6. Knockdown efficiency of MAFF, BTG3, and NOXA siRNA. Supplementary Fig. 7. NOXA played a critical role in combination treatment-induced apoptosis in NSCLC tumor spheroids. Supplementary Fig. 8. Apoptosis induced by the upregulation of NOXA in response to the combination treatment was preferentially mediated by MCL1 rather than survivin. Supplementary Fig. 9. Treatment with narciclasine both alone and in combination with cisplatin increased $H_2O_2$ levels. Supplementary Fig. 10. p53 expression and cleavage of caspase-7 increased after 24 h of treatment with cisplatin and narciclasine.

**Acknowledgements**

Natural products were kindly provided by the Natural Product Bank at the National Institute of Korean Oriental Medicine (NIKOM).

**Author contributions**

J.H.L. performed in vitro and in vivo experiments with the interpretation of results and bioinformatic analyses with validation, and wrote the original manuscript. S.H.S. performed the cycloheximide chase experiment and wrote the manuscript. J.S. conceived the study, designed experiments, and edited the manuscript. Y.-N.K. managed the research project, conceived the study, and edited the manuscript. K.Y. conceived the study, acquired funding, designed the experiments, analyzed the results, and wrote the manuscript. All authors read and approved the final manuscript.

**Funding**

This research was supported by National Cancer Center research grants 2110262 and 2310670.

**Availability of data and materials**

The datasets generated or analyzed during the current study are included in this published article and the supplementary information files. Data not included are available from the corresponding author upon request.

## Declarations

**Ethics approval and consent to participate**
Animal experiments were reviewed and approved by the Institutional Animal Care and Use Committee (IACUC) of National Cancer Center Research Institute (NCCRI, approval no. NCC-23-884), and the IACUC of NCCRI follows the rules of Basel Declaration. NCCRI is an Association for Assessment and Accreditation of Laboratory Animal Care International (AAALAC International)-accredited facility and abides by the Institute of Laboratory Animal Resources (ILAR) guide.

**Consent for publication**
Not applicable.

**Competing interests**
The authors declare that they have no competing interests.

Received: 24 October 2024 Accepted: 22 April 2025
Published online: 14 May 2025

**References**

1. Siegel RL, Miller KD, Wagle NS, Jemal A. Cancer statistics, 2023. CA Cancer J Clin. 2023;73(1):17–48.
2. SEER*Explorer: An interactive website for SEER cancer statistics. Surveillance Research Program, National Cancer Institute, Data source(s): SEER Incidence Data, November 2022 Submission (1975–2020), SEER 22 registries, 2023. 2023. https://seer.cancer.gov/statistics-network/explorer/. Accessed 31 Mar 2024.
3. Thai AA, Solomon BJ, Sequist LV, Gainor JF, Heist RS. Lung cancer. Lancet. 2021;398(10299):535–54.
4. Liu SM, Zheng MM, Pan Y, Liu SY, Li Y, Wu YL. Emerging evidence and treatment paradigm of non-small cell lung cancer. J Hematol Oncol. 2023;16(1):40.
5. Daly ME, Singh N, Ismaila N, Antonoff MB, Arenberg DA, Bradley J, et al. Management of stage III non-small-cell lung cancer: ASCO guideline. J Clin Oncol. 2022;40(12):1356–84.
6. Singh N, Temin S, Baker S Jr, Blanchard E, Brahmer JR, Celano P, et al. Therapy for stage IV non-small-cell lung cancer with driver alterations: ASCO living guideline. J Clin Oncol. 2022;40(28):3310–22.
7. Singh N, Temin S, Baker S Jr, Blanchard E, Brahmer JR, Celano P, et al. Therapy for stage IV non-small-cell lung cancer without driver alterations: ASCO living guideline. J Clin Oncol. 2022;40(28):3323–43.
8. Hendriks LE, Kerr KM, Menis J, Mok TS, Nestle U, Passaro A, et al. Non-oncogene-addicted metastatic non-small-cell lung cancer: ESMO Clinical Practice Guideline for diagnosis, treatment and follow-up. Ann Oncol. 2023;34(4):358–76.
9. Hendriks LE, Kerr KM, Menis J, Mok TS, Nestle U, Passaro A, et al. Oncogene-addicted metastatic non-small-cell lung cancer: ESMO Clinical Practice Guideline for diagnosis, treatment and follow-up. Ann Oncol. 2023;34(4):339–57.
10. Araghi M, Mannani R, Heidarnejad Maleki A, Hamidi A, Rostami S, Safa SH, et al. Recent advances in non-small cell lung cancer targeted therapy; an update review. Cancer Cell Int. 2023;23(1):162.
11. Abu Rous F, Singhi EK, Sridhar A, Faisal MS, Desai A. Lung cancer treatment advances in 2022. Cancer Invest. 2023;41(1):12–24.
12. Ali R, Aouida M, Alhaj Sulaiman A, Madhusudan S, Ramotar D. Can cisplatin therapy be improved? Pathways that can be targeted. Int J Mol Sci. 2022;23(13):7241.
13. Fennell DA, Summers Y, Cadranel J, Benepal T, Christoph DC, Lal R, et al. Cisplatin in the modern era: the backbone of first-line chemotherapy for non-small cell lung cancer. Cancer Treat Rev. 2016;44:42–50.
14. Huang M, Lu JJ, Ding J. Natural products in cancer therapy: past, present and future. Nat Prod Bioprospect. 2021;11(1):5–13.
15. Fürst R. Narciclasine—an *Amaryllidaceae* alkaloid with potent antitumor and anti-inflammatory properties. Planta Med. 2016;82(16):1389–94.
16. Dumont P, Ingrassia L, Rouzeau S, Ribaucour F, Thomas S, Roland I, et al. The *Amaryllidaceae isocarbostyril* narciclasine induces apoptosis by activation of the death receptor and/or mitochondrial pathways in cancer cells but not in normal fibroblasts. Neoplasia. 2007;9(9):766–76.
17. Yuan Y, He X, Li X, Liu Y, Tang Y, Deng H, et al. Narciclasine induces autophagy-mediated apoptosis in gastric cancer cells through the Akt/mTOR signaling pathway. BMC Pharmacol Toxicol. 2021;22(1):70.
18. Van Goietsenoven G, Mathieu V, Lefranc F, Kornienko A, Evidente A, Kiss R. Narciclasine as well as other *Amaryllidaceae isocarbostyrils* are promising GTP-ase targeting agents against brain cancers. Med Res Rev. 2013;33(2):439–55.
19. Van Goietsenoven G, Hutton J, Becker JP, Lallemand B, Robert F, Lefranc F, et al. Targeting of eEF1A with *Amaryllidaceae isocarbostyrils* as a strategy to combat melanomas. FASEB J. 2010;24(11):4575–84.
20. Lv C, Huang Y, Huang R, Wang Q, Zhang H, Jin J, et al. Narciclasine targets STAT3 via distinct mechanisms in tamoxifen-resistant breast cancer cells. Mol Ther Oncolytics. 2022;24:340–54.
21. Oda E, Ohki R, Murasawa H, Nemoto J, Shibue T, Yamashita T, et al. Noxa, a BH3-only member of the Bcl-2 family and candidate mediator of p53-induced apoptosis. Science. 2000;288(5468):1053–8.
22. Singh R, Letai A, Sarosiek K. Regulation of apoptosis in health and disease: the balancing act of BCL-2 family proteins. Nat Rev Mol Cell Biol. 2019;20(3):175–93.
23. Strasser A, Cory S, Adams JM. Deciphering the rules of programmed cell death to improve therapy of cancer and other diseases. EMBO J. 2011;30(18):3667–83.
24. Roufayel R, Younes K, Al-Sabi A, Murshid N. BH3-only proteins Noxa and Puma are key regulators of induced apoptosis. Life. 2022;12(2):256.

25. Gomez-Bougie P, Ménoret E, Juin P, Dousset C, Pellat-Deceunynck C, Amiot M. Noxa controls Mule-dependent Mcl-1 ubiquitination through the regulation of the Mcl-1/USP9X interaction. Biochem Biophys Res Commun. 2011;413(3):460–4.
26. Arai S, Varkaris A, Nouri M, Chen S, Xie L, Balk SP. MARCH5 mediates NOXA-dependent MCL1 degradation driven by kinase inhibitors and integrated stress response activation. Elife. 2020;9: e54954.
27. Nakajima W, Sharma K, Lee JY, Maxim NT, Hicks MA, Vu TT, et al. DNA damaging agent-induced apoptosis is regulated by MCL-1 phosphorylation and degradation mediated by the Noxa/MCL-1/CDK2 complex. Oncotarget. 2016;7(24):36353–65.
28. Wang H, Guo M, Wei H, Chen Y. Targeting MCL-1 in cancer: current status and perspectives. J Hematol Oncol. 2021;14(1):67.
29. Mei Y, Xie C, Xie W, Tian X, Li M, Wu M. Noxa/Mcl-1 balance regulates susceptibility of cells to camptothecin-induced apoptosis. Neoplasia. 2007;9(10):871–81.
30. Sharma K, Vu TT, Cook W, Naseri M, Zhan K, Nakajima W, et al. p53-independent Noxa induction by cisplatin is regulated by ATF3/ATF4 in head and neck squamous cell carcinoma cells. Mol Oncol. 2018;12(6):788–98.
31. Guikema JE, Amiot M, Eldering E. Exploiting the pro-apoptotic function of NOXA as a therapeutic modality in cancer. Expert Opin Ther Targets. 2017;21(8):767–79.
32. Yang M, Lu Y, Piao W, Jin H. The translational regulation in mTOR pathway. Biomolecules. 2022;12(6):802.
33. Pakos-Zebrucka K, Koryga I, Mnich K, Ljujic M, Samali A, Gorman AM. The integrated stress response. EMBO Rep. 2016;17(10):1374–95.
34. Urano F, Wang X, Bertolotti A, Zhang Y, Chung P, Harding HP, et al. Coupling of stress in the ER to activation of JNK protein kinases by transmembrane protein kinase IRE1. Science. 2000;287(5453):664–6.
35. Siwecka N, Rozpedek-Kaminska W, Wawrzynkiewicz A, Pytel D, Diehl JA, Majsterek I. The structure, activation and signaling of IRE1 and its role in determining cell fate. Biomedicines. 2021;9(2):156.
36. Harding HP, Novoa I, Zhang Y, Zeng H, Wek R, Schapira M, et al. Regulated translation initiation controls stress-induced gene expression in mammalian cells. Mol Cell. 2000;6(5):1099–108.
37. Zhang Z, Zhang L, Zhou L, Lei Y, Zhang Y, Huang C. Redox signaling and unfolded protein response coordinate cell fate decisions under ER stress. Redox Biol. 2019;25: 101047.
38. Yokouchi M, Hiramatsu N, Hayakawa K, Okamura M, Du S, Kasai A, et al. Involvement of selective reactive oxygen species upstream of proapoptotic branches of unfolded protein response. J Biol Chem. 2008;283(7):4252–60.
39. Kadara H, Lacroix L, Lotan D, Lotan R. Induction of endoplasmic reticulum stress by the pro-apoptotic retinoid N-(4-hydroxyphenyl)retinamide via a reactive oxygen species-dependent mechanism in human head and neck cancer cells. Cancer Biol Ther. 2007;6(5):705–11.
40. Almanza A, Carlesso A, Chintha C, Creedican S, Doultsinos D, Leuzzi B, et al. Endoplasmic reticulum stress signaling—from basic mechanisms to clinical applications. FEBS J. 2019;286(2):241–78.
41. Nishitoh H, Matsuzawa A, Tobiume K, Saegusa K, Takeda K, Inoue K, et al. ASK1 is essential for endoplasmic reticulum stress-induced neuronal cell death triggered by expanded polyglutamine repeats. Genes Dev. 2002;16(11):1345–55.
42. Hung JH, Su IJ, Lei HY, Wang HC, Lin WC, Chang WT, et al. Endoplasmic reticulum stress stimulates the expression of cyclooxygenase-2 through activation of NF-kappaB and pp38 mitogen-activated protein kinase. J Biol Chem. 2004;279(45):46384–92.
43. Zhao Q, Bi Y, Guo J, Liu Y, Zhong J, Liu Y, et al. Effect of pristimerin on apoptosis through activation of ROS/endoplasmic reticulum (ER) stress-mediated noxa in colorectal cancer. Phytomedicine. 2021;80: 153399.
44. Kovarik P, Stoiber D, Eyers PA, Menghini R, Neininger A, Gaestel M, et al. Stress-induced phosphorylation of STAT1 at Ser727 requires p38 mitogen-activated protein kinase whereas IFN-gamma uses a different signaling pathway. Proc Natl Acad Sci USA. 1999;96(24):13956–61.
45. Zhang Y, Cho YY, Petersen BL, Zhu F, Dong Z. Evidence of STAT1 phosphorylation modulated by MAPKs, MEK1 and MSK1. Carcinogenesis. 2004;25(7):1165–75.
46. Costa EC, Moreira AF, de Melo-Diogo D, Gaspar VM, Carvalho MP, Correia IJ. 3D tumor spheroids: an overview on the tools and techniques used for their analysis. Biotechnol Adv. 2016;34(8):1427–41.
47. Sant S, Johnston PA. The production of 3D tumor spheroids for cancer drug discovery. Drug Discov Today Technol. 2017;23:27–36.
48. Muguruma M, Teraoka S, Miyahara K, Ueda A, Asaoka M, Okazaki M, et al. Differences in drug sensitivity between two-dimensional and three-dimensional culture systems in triple-negative breast cancer cell lines. Biochem Biophys Res Commun. 2020;533(3):268–74.
49. Liang SQ, Bührer ED, Berezowska S, Marti TM, Xu D, Froment L, et al. mTOR mediates a mechanism of resistance to chemotherapy and defines a rational combination strategy to treat KRAS-mutant lung cancer. Oncogene. 2019;38(5):622–36.
50. Lee JH, Park SY, Hwang W, Sung JY, Cho ML, Shim J, et al. Isoharringtonine induces apoptosis of non-small cell lung cancer cells in tumorspheroids via the intrinsic pathway. Biomolecules. 2020;10(11):1521.
51. Tate JG, Bamford S, Jubb HC, Sondka Z, Beare DM, Bindal N, et al. COSMIC: the catalogue of somatic mutations in cancer. Nucleic Acids Res. 2018;47(D1):D941–7.
52. Wang Q, Mora-Jensen H, Weniger MA, Perez-Galan P, Wolford C, Hai T, et al. ERAD inhibitors integrate ER stress with an epigenetic mechanism to activate BH3-only protein NOXA in cancer cells. Proc Natl Acad Sci USA. 2009;106(7):2200–5.
53. Kim JY, Ahn HJ, Ryu JH, Suk K, Park JH. BH3-only protein Noxa is a mediator of hypoxic cell death induced by hypoxia-inducible factor 1alpha. J Exp Med. 2004;199(1):113–24.
54. Flinterman M, Guelen L, Ezzati-Nik S, Killick R, Melino G, Tominaga K, et al. E1A activates transcription of p73 and Noxa to induce apoptosis. J Biol Chem. 2005;280(7):5945–59.
55. Nakajima W, Miyazaki K, Asano Y, Kubota S, Tanaka N. Krüppel-like factor 4 and its activator APTO-253 induce NOXA-mediated, p53-independent apoptosis in triple-negative breast cancer cells. Genes. 2021;12(4):539.
56. Ku HC, Cheng CF. Master regulator activating transcription factor 3 (ATF3) in metabolic homeostasis and cancer. Front Endocrinol. 2020;11:556.

57. Yan C, Lu D, Hai T, Boyd DD. Activating transcription factor 3, a stress sensor, activates p53 by blocking its ubiquitination. EMBO J. 2005;24(13):2425–35.
58. Li X, Zhou X, Li Y, Zu L, Pan H, Liu B, et al. Activating transcription factor 3 promotes malignance of lung cancer cells in vitro. Thorac Cancer. 2017;8(3):181–91.
59. Ham B, Fernandez MC, D'Costa Z, Brodt P. The diverse roles of the TNF axis in cancer progression and metastasis. Trends Cancer Res. 2016;11(1):1–27.
60. Albert MC, Brinkmann K, Pokrzywa W, Günther SD, Krönke M, Hoppe T, et al. CHIP ubiquitylates NOXA and induces its lysosomal degradation in response to DNA damage. Cell Death Dis. 2020;11(9):740.
61. Brinkmann K, Zigrino P, Witt A, Schell M, Ackermann L, Broxtermann P, et al. Ubiquitin C-terminal hydrolase-L1 potentiates cancer chemosensitivity by stabilizing NOXA. Cell Rep. 2013;3(3):881–91.
62. Aikawa T, Shinzawa K, Tanaka N, Tsujimoto Y. Noxa is necessary for hydrogen peroxide-induced caspase-dependent cell death. FEBS Lett. 2010;584(4):681–8.
63. Willis SN, Chen L, Dewson G, Wei A, Naik E, Fletcher JI, et al. Proapoptotic Bak is sequestered by Mcl-1 and Bcl-xL, but not Bcl-2, until displaced by BH3-only proteins. Genes Dev. 2005;19(11):1294–305.
64. Nakajima W, Hicks MA, Tanaka N, Krystal GW, Harada H. Noxa determines localization and stability of MCL-1 and consequently ABT-737 sensitivity in small cell lung cancer. Cell Death Dis. 2014;5(2): e1052.
65. Senichkin VV, Streletskaia AY, Gorbunova AS, Zhivotovsky B, Kopeina GS. Saga of Mcl-1: regulation from transcription to degradation. Cell Death Differ. 2020;27(2):405–19.
66. Zhang S, Zhang M, Jing Y, Yin X, Ma P, Zhang Z, et al. Deubiquitinase USP13 dictates MCL1 stability and sensitivity to BH3 mimetic inhibitors. Nat Commun. 2018;9(1):215.
67. Shoemaker RH. The NCI60 human tumour cell line anticancer drug screen. Nat Rev Cancer. 2006;6(10):813–23.
68. Pettit GR, Pettit GR, Backhaus RA, Boyd MR, Meerow AW. Antineoplastic agents, 256. Cell growth inhibitory isocarbostyrils from *Hymenocallis*. J Nat Prod. 1993;56(10):1682–7.
69. Hu H, Tian M, Ding C, Yu S. The C/EBP homologous protein (CHOP) transcription factor functions in endoplasmic reticulum stress-induced apoptosis and microbial infection. Front Immunol. 2018;9:3083.
70. Townsend PA, Scarabelli TM, Davidson SM, Knight RA, Latchman DS, Stephanou A. STAT-1 interacts with p53 to enhance DNA damage-induced apoptosis. J Biol Chem. 2004;279(7):5811–20.


## Publisher's Note